https://doi.org/10.5194/egusphere-2026-2566
Preprint. Discussion started: 8 May 2026

Estimating cross-stream isopycnal eddy diffusivity from mooring observations

Miriam F. Sterl[1,2], Carlo J. Mans[3], Alberto C. Naveira Garabato[4], and Sjoerd Groeskamp[1]

[1]Department of Ocean Systems, Royal Netherlands Institute for Sea Research, Texel, The Netherlands
[2]Institute for Marine and Atmospheric Research, Utrecht University, Utrecht, The Netherlands
[3]Geophysical Institute, University of Bergen and Bjerknes Centre for Climate Research, Bergen, Norway
[4]Ocean and Earth Science, University of Southampton, Southampton, United Kingdom

Correspondence: Miriam F. Sterl (miriam.sterl@mpimet.mpg.de)

Abstract. We present a method to derive distributions of cross-stream isopycnal eddy diffusivities in the Antarctic Circumpolar Current (ACC) from data measured by a mooring. This method transforms the time series measured by the mooring to spatial (cross-stream) distributions using dynamic height as the cross-stream coordinate. For this transformation, the relation between dynamic height and cross-stream location must be inferred from a spatial data set, such as hydrographic section measurements or reanalysis data along a transect through the mooring. From the distribution of temperature as a function of neutral density and cross-stream distance, the isopycnal temperature properties and fluctuations can be determined, and a mixing length and eddy diffusivity can be inferred. We apply this method to a mooring in Drake Passage and compare the resulting distributions with those derived from hydrographic section data. The mooring and section data yield very similar distributions of the mean isopycnal temperature field as well as the root mean square (rms) temperature fluctuations along isopycnals, which provide a metric of isopycnal stirring. The mooring-derived eddy diffusivity distributions capture some key features predicted by kinematic theories: reduced diffusivities at the Sub-Antarctic Front jet and increased diffusivities at mid-depths, both in line with mean flow suppression theory. The results presented here show that the methodology can be a valuable tool to study cross-stream isopycnal mixing properties from mooring data, especially in equivalent-barotropic systems and for moorings with a high vertical resolution.

1 Introduction

The Southern Ocean is a key site of global ocean mixing and contributes to the redistribution of heat, nutrients, and other water mass properties (e.g. Rintoul, 2018; Newman et al., 2019; Sallée et al., 2025). Southern Ocean dynamics are driven by dominant westerly winds as well as buoyancy forcing (Rintoul and Naveira Garabato, 2013; Howard et al., 2015). The strong winds create an Ekman circulation and act to steepen the isopycnals. This overturning of isopycnals is thought to be balanced by the influence of geostrophic eddies which flatten the isopycnals. Thus, the overturning circulation in the Southern Ocean can be seen as the resultant flow of two dynamically intertwined circulatory systems: a wind-driven Ekman circulation and an eddy circulation driven by geostrophic turbulence (Olbers and Visbeck, 2005; Marshall and Radko, 2006; Abernathey et al., 2011; Marshall and Speer, 2012). In the latter case, mesoscale dynamics play a leading role in the eddy stirring responsible for

https://doi.org/10.5194/egusphere-2026-2566
Preprint. Discussion started: 8 May 2026

driving the overturning circulation (Kusters et al., 2025). Hence, accurate portrayals of the mesoscale field in both theoretical and quantitative terms are critical for an accurate description of Southern Ocean dynamics (Gille et al., 2022).

The rate of stirring by mesoscale eddies along isopycnals is typically characterised by an isopycnal eddy diffusivity, $\mathcal{K}$. A distinction can be made between buoyancy diffusivity, which describes an eddy induced advection resembling diffusion of buoyancy (Gent and McWilliams, 1990; Gent et al., 1995; McDougall and McIntosh, 2001; Young, 2012), and tracer diffusivity representing fluxes of tracers along isopycnals (Redi, 1982; Griffies, 1998). Here we focus on isopycnal tracer diffusivity. In global ocean and climate models that do not resolve the mesoscale (10–100 km), the isopycnal tracer diffusivity is often used to parametrise tracer fluxes induced by eddy stirring via a flux-gradient relation, relating the tracer flux $\mathcal{F}_C$ to the large-scale isopycnal tracer gradient $\nabla_n C$ as $\mathcal{F}_C = -\mathcal{K}\nabla_n C$. The results of climate and ocean models can be greatly affected by the choice of the eddy diffusivity value (Pradal and Gnanadesikan, 2014; Gnanadesikan et al., 2015; Jones and Abernathey, 2019; Chouksey et al., 2022; Holmes et al., 2022). Adequate parameterisations thus require robust and widespread estimates of the eddy diffusivity. This is of particular importance for high latitudes, including large parts of the Southern Ocean, because the deformation radius becomes so small that even high resolution ocean models may not fully resolve mesoscale eddies (Hewitt et al., 2020).

Direct observations of the eddy diffusivity can be made using tracer release experiments (e.g. Ledwell et al., 1993, 1998) or float-based experiments, such as those conducted during the Diapycnal and Isopycnal Mixing Experiment in the Southern Ocean (DIMES; e.g. Tulloch et al., 2014; LaCasce et al., 2014). While providing a ground truth for eddy diffusivities, these studies are rare and apply to only a small region of the ocean. Many studies therefore focus on indirect estimates using a wide range of approaches, for example using satellite data (Abernathey and Marshall, 2013; Busecke and Abernathey, 2019), inverse methods (Zika et al., 2010; Groeskamp et al., 2014, 2017; Kusters et al., 2024) or hydrographic data (Cole et al., 2015; Roach et al., 2016, 2018; Chapman and Sallée, 2017; Meneghello et al., 2017; Groeskamp et al., 2020; Sévellec et al., 2022). As part of the DIMES experiment, Naveira Garabato et al. (2011) (hereafter NG11) proposed a method to estimate eddy diffusivities from hydrographic sections across the Southern Ocean. Their methodology is based on an extension of mixing length theory (Prandtl, 1925), estimating a mixing length from temperature fluctuations and gradients along neutral surfaces (Armi and Stommel, 1983). Notably, their results corroborate theoretical work suggesting suppression of eddy stirring in the cores of ocean jets, resulting from modulation of the mixing length by eddy-mean flow interactions (Ferrari and Nikurashin, 2010; Klocker et al., 2012). In this study we estimate cross-stream eddy diffusivities across the Antarctic Circumpolar Current (ACC) by extending the method presented in NG11 to observational data provided by a mooring located in Drake Passage. We show that we can use mooring timeseries to represent cross-stream profiles and derive spatial distributions of $\mathcal{K}$. This transformation from temporal to spatial data makes use of the hydrographic section measurements; in addition, we show that it is also possible to use readily available data sets such as reanalysis products instead, such that ship-based transects are not needed and this method can potentially be applied to other moorings.

The paper is organised as follows. Section 2 provides relevant theoretical background information, including a description of the methodology of NG11. Section 3 presents the different data sets used in this study. In Section 4, we describe our methodology for estimating eddy diffusivities from mooring data. Section 5 presents the results, comparing the hydrographic

https://doi.org/10.5194/egusphere-2026-2566
Preprint. Discussion started: 8 May 2026

section data with the mooring data, and comparing the diffusivity distributions calculated from the mooring data with other diffusivity data sets. Section 6 discusses both the methodology and the resulting diffusivity distributions we find in Drake Passage. Final remarks and conclusions are given in Section 7.

2 Theoretical background

2.1 Mixing length theory

Commonly, the eddy diffusivity $\mathcal{K}$ is parametrised via mixing length theory (Prandtl, 1925):

$$\mathcal{K} = \Gamma U_e L_{\text{mix}}. \tag{1}$$

Here Γ represents an empirically determined, non-dimensional mixing efficiency, U_e (m s^{-1}) is an eddy velocity scale, and L_{mix} (m) is the mixing length. The eddy velocity scale quantifies the magnitude of velocity fluctuations caused by turbulent eddies and characterises their intensity, while the mixing length is a measure of the distance over which an eddy carries the value of a conservative tracer, before it is mixed with its environment (Ferrari and Polzin, 2005). In other words, it is the distance over which eddies can effectively mix tracers.

Armi and Stommel (1983) proposed an estimate of the mixing length scale, based on the observed variance of a tracer c (in their case, salinity):

$$L_{\text{mix}} = \frac{c_{\text{rms}}}{|\nabla_n \overline{c}|}, \tag{2}$$

where c_{rms} is the root mean squared (rms) tracer fluctuation along a neutral surface (isopycnal) arising from eddy stirring of the large-scale tracer concentration $\overline{c}$, and $\nabla_n \overline{c}$ is the isopycnal gradient of the large-scale tracer field. This definition of the mixing length holds only under the assumptions that the gradient does not vary significantly over the mixing length (i.e. there is a scale separation between the eddy and mean flow scales) and that the temperature fluctuations are generated locally, not transported in from regions upstream. Equation (2) can be applied to hydrographic temperature and salinity measurements to infer diffusivities. This was done for example by Ferrari and Polzin (2005) for the North Atlantic and by NG11 and Naveira Garabato et al. (2016) for the Antarctic Circumpolar Current, using temperature as a tracer. Cole et al. (2015) even used (2) considering salinity as tracer to derive the first global maps of eddy diffusivity for the upper 2000 m of the ocean.

2.2 Eddy diffusivity estimate of NG11

NG11 used (1) and (2) to estimate cross-stream distributions of eddy diffusivities from hydrographic section data, using temperature (Θ) as a tracer to estimate the mixing length:

$$L_{\text{mix}} = \frac{\Theta_{\text{rms}}}{|\nabla_n \overline{\Theta}|}. \tag{3}$$

They were interested in the cross-stream eddy diffusivity, hence they took U_e to be a cross-stream eddy velocity scale, and considered cross-stream temperature gradients on neutral surfaces in the calculation of L_{mix}.

https://doi.org/10.5194/egusphere-2026-2566
Preprint. Discussion started: 8 May 2026

The first important ingredient of their methodology was defining an appropriate cross-stream distance metric. Meandering of the ACC streamlines may introduce temperature anomalies at a fixed location which are reversible and do not directly imply cross-stream mixing. To isolate temperature anomalies associated with cross-stream mixing, NG11 proposed to use as cross-stream coordinate a baroclinic streamfunction, representing the ACC streamlines. Specifically, they used the dynamic height anomaly at 500 dbar relative to 1500 dbar:

$$\phi_{500}^{1500} = \int_{500}^{1500} \delta \, \mathrm{d}p, \tag{4}$$

where δ ($\mathrm{m}^3\ \mathrm{kg}^{-1}$) is the specific volume anomaly and p (dbar) is pressure. The exact choice of pressure reference level does not impact the results, because the ACC streamlines are equivalent barotropic and hence show little variation with depth (see Appendix A in NG11). The magnitude of ϕ_{500}^{1500} provides insight into the vertical proximity of density contours, thus relating to the strength of currents and eddying motions. NG11 determined a relationship between ϕ_{500}^{1500} and the along-section distance of the stations (relative to the southernmost station) by fitting a cubic spline to the measured data points of the section. This spline fit yields a cross-stream pseudo-distance, Y, for each hydrographic section profile. By using this pseudo-distance defined in terms of the dynamic height, the effect of meandering of streamlines is filtered out. The cross-stream temperature gradients on neutral surfaces in (3) are then computed as derivatives with respect to Y: $\nabla_n = \partial_n / \partial Y$. This resembles the projected non-orthogonal approach that is a good approximation to the exact gradient (McDougall et al., 2014).

Next, they needed the temperature data from the hydrographic sections on neutral surfaces rather than pressure surfaces. Hence, they sorted the temperature data into neutral density bins, and then fitted a spline relating Y to Θ on every neutral surface. This spline denotes the large scale $\overline{\Theta}(Y)$, being smooth, continuous and differentiable, as required for computing $\partial_n \overline{\Theta} / \partial Y$. The rms temperature Θ_{rms} was then estimated as the standard deviation of $\Theta - \overline{\Theta}(Y)$ for all measurements within a window $Y \pm \Delta Y$. Thus, the mixing length could be computed via (3).

With the mixing length computed, the final ingredient for calculating the eddy diffusivity is the cross-stream eddy velocity scale U_e (Equation 1). As the hydrographic section data does not include velocity measurements, NG11 instead derived U_e from altimetry data.

2.3 Suppression theory

The eddy diffusivity estimate of NG11 is based on isopycnal gradients and fluctuations of temperature. We can thus consider it as a hydrographic or thermodynamic approach to computing eddy diffusivity. However, there are other methods of deriving eddy diffusivity based on kinematic or dynamical approaches. One important example of such a method is the estimate derived by Ferrari and Nikurashin (2010) and Klocker et al. (2012). They find that cross-stream eddy diffusivities are suppressed in regions with strong mean flows if the eddies are propagating relative to the mean flow. This can be interpreted as the mean flow advecting tracers through the eddy field before the eddies have had time to effectively mix tracers in the cross-stream direction. An alternative interpretation is based on the potential vorticity (PV) gradient, as it is the PV gradient that enables the eddies to move relative to the mean flow; a cross-stream mixing barrier is related to a strong PV gradient (Nakamura and Zhu,

https://doi.org/10.5194/egusphere-2026-2566
Preprint. Discussion started: 8 May 2026

2010; Srinivasan and Young, 2014; Balwada et al., 2016; Sterl et al., 2024). In their studies, Ferrari and Nikurashin (2010) and Klocker et al. (2012) derived the following expression for the cross-stream eddy diffusivity:

$$\mathcal{K} = \frac{\mathcal{K}_0}{1 + k^2\gamma^{-2}\left(c_w - U\right)^2}, \tag{5}$$

where k is the zonal eddy wavenumber, γ an inverse eddy decorrelation timescale, U the mean flow velocity, c_w the eddy phase speed relative to the ground, and $\mathcal{K}_0$ the 'unsuppressed diffusivity' for eddies moving with the mean flow ($c_w - U = 0$). This expression has been validated and applied to the ACC in multiple studies (Sallée et al., 2011; Meredith et al., 2012; Pennel and Kamenkovich, 2014; Chen et al., 2015; Roach et al., 2016).

3 Data

3.1 Hydrographic sections

We use data from repeat hydrographic sections taken as part of the World Ocean Circulation (WOCE) experiment in the eastern Drake Passage (section SR1b; Figure 1). This data was also used by NG11. The section repeats were taken between 1993–2005; exact dates can be found in Table 1 of NG11. In total, the data set includes 316 profiles from 10 different transects. The data set spans a depth range from the surface to a maximum of 4850 dbar, depending on location, with a vertical resolution of 2 dbar. We convert measurements of in-situ temperature and practical salinity to conservative temperature (Θ; McDougall, 2003), absolute salinity (S_A; McDougall et al., 2012), and neutral density (γ^n; Jackett and McDougall, 1997) using the TEOS-10 software (McDougall and Barker, 2011). From now on, unless explicitly mentioned otherwise, the terms salinity, temperature and density will refer to S_A, Θ and γ^n, respectively. Note that NG11 considered potential temperature instead of conservative temperature in their calculations.

3.2 Mooring

Subsequently, we make use of observational data stemming from a mooring located in Drake passage (Brearley et al., 2013; Sévellec et al., 2015; Cusack et al., 2020). An array of moorings was deployed as part of the DIMES project. The array consists of 5 moorings in a cross configuration (Figure 1), deployed on 18–20 December 2010 and recovered on 5–6 March 2012. They were equipped with Nortek acoustic current meters and Seabird Electronics SBE37 Microcat CTDs, providing measurements of horizontal velocity u, v and in-situ temperature and practical salinity T, S, respectively, with a resolution of 15 minutes. The centre mooring measured these variables at 12 nominal depth levels (425, 475, 525, 575, 1200, 1299, 1853, 1951, 2049, 2152, 3400, 3600 m), while the other moorings measured at 5 depth levels (Sévellec et al., 2015). We will use the data of the centre mooring only, because the low vertical resolution of the other moorings is insufficient to capture relevant smaller-scale temperature variations (Ferrari and Polzin, 2005). From now on, when referring to 'the mooring', the centre mooring of the DIMES array is implied (indicated with a 'C' in the inset of Figure 1).

As for the hydrographic section data, we convert T and S to Θ and S_A and compute the neutral density γ^n. We down-sample the mooring data from values every 15 minutes to daily values by taking daily averages for all variables, resulting in

https://doi.org/10.5194/egusphere-2026-2566
Preprint. Discussion started: 8 May 2026

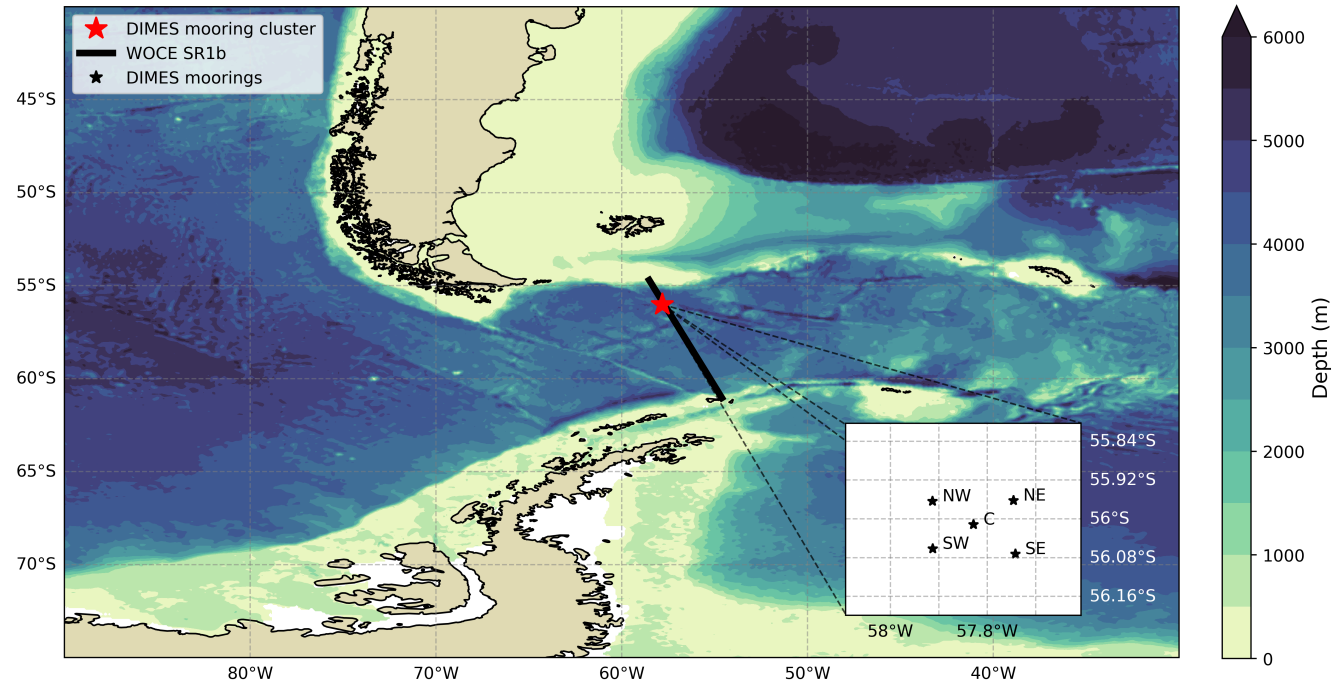

Figure 1. Geographical overview of the Southern Ocean region of interest, featuring the locations of DIMES moorings denoted by a red marker and the WOCE SR1b hydrographic section in black. The inset shows the configuration of the individual moorings of the DIMES array. Topography is taken from the GLORYS12V1 data set.

a total of 438 profiles. We do this to average out near- and super-inertial variability that we expect to be unrelated to eddy stirring. Further, we interpolate values between the bottom and top measurement using a Multiply-Rotated Piecewise Cubic Hermite Interpolating Polynomials (MR-PCHIP) scheme (Barker and McDougall, 2020). This interpolation scheme has the advantage of avoiding unrealistic overshoots compared to conventional methods. We interpolate such that we have samples of $u, v, \Theta, S_A, \gamma^n$ at intervals of 10 dbar.

3.3 Reanalysis products and climatologies

As we will see in the next section, we will need a spatial data set to define a cross-stream coordinate for the mooring profiles. In addition to the hydrographic section data, we make use of a few other global data products to extract monthly temperature data along the SR1b section. The first is the Roemmich-Gilson Argo climatology (Roemmich and Gilson, 2009), which provides data for the upper ocean based on profiling floats from the Argo Program. The second product is GLORYS12V1 (hereafter GLORYS), the E.U. Copernicus Marine Service Information (CMEMS) global ocean eddy-resolving reanalysis, using the NEMO model component driven at the surface by ECMWF ERA-Interim then ERA5 reanalyses for recent years. Finally, we use the Southern Ocean State Estimate (SOSE), a model-generated best fit to Southern Ocean observations, using the MITgcm

https://doi.org/10.5194/egusphere-2026-2566
Preprint. Discussion started: 8 May 2026

Data set	Time period	Grid resolution	Max depth	Nr of depth levels
Argo	2010–2012	1°	2000 dbar	58
GLORYS	2010–2012	1/12°	5728 m	50
SOSE	2013–2015	1/6°	5800 m	52

Table 1. Temporal and spatial properties of the Argo, GLORYS and SOSE data sets.

(Mazloff et al., 2010). Table 1 gives an overview of the horizontal and vertical resolutions of these three data products, as well as the time periods that we selected from each one. For the Argo and GLORYS data, we select the years that overlap with the mooring timeseries. The newest SOSE run is only available for 2013 onwards, so we select the first three years of that period.

3.4 Other diffusivity data sets

We will compare our computed eddy diffusivities to diffusivity distributions from other data sets. Specifically, we will use the data from Chapman and Sallée (2017) (hereafter CS17) and from Groeskamp et al. (2020) (hereafter G20). Both studies compute diffusivity estimates from suppression theory, equation (5). The different assumptions, data sources and computations employed in CS17 and G20 to apply equation (5) are summarised in Table 2. Aside from the usage of different data sets, the main methodological difference between both studies is in the computation of the unsuppressed diffusivity $\mathcal{K}_0$. Here, CS17 uses an expression based on the rms geostrophic streamfunction fluctuations (Holloway, 1986; Keffer and Holloway, 1988). G20 derives $\mathcal{K}_0$ from mixing length theory (Prandtl, 1925) and uses a vertical structure function to extend the estimates to full-depth diffusivity profiles (De La Lama et al., 2016; LaCasce and Groeskamp, 2020).

4 Methodology

We apply the methodology of NG11 as summarised in Section 2.2 to both hydrographic section and mooring data, adapting it to work for mooring data where necessary. In this section, we give a detailed description of our approach and the differences and similarities with NG11.

4.1 Cross-stream distance metric

First, we need to compute ϕ_{500}^{1500} and from that define the cross-stream pseudo-distance Y. For the hydrographic section data, we determine a relationship between ϕ_{500}^{1500} and the along-section distance of the stations (relative to the southernmost station) by fitting a cubic spline to the measured data points (Figure 2a), using the Python package `csaps`. However, fitting a cross-stream distance metric is not possible for the mooring, because it is at a fixed geographical location. Instead, we will use the fitted relation between ϕ_{500}^{1500} and Y determined from the SR1b section on the mooring data, since the mooring was situated in the region sampled by the SR1b hydrographic section (Figure 1). Figure 3 shows the measured profiles from the SR1b section and the mooring as a function of ϕ_{500}^{1500}. Despite some differences, there is good agreement between the two data sets, motivating

https://doi.org/10.5194/egusphere-2026-2566
Preprint. Discussion started: 8 May 2026

	CS17	**G20**
Grid resolution	$1/4°$	$1°$
Max depth	1975 m	5500 m
Hydrographic data	Argo profiles taken between 1 January 2006 and 31 December 2014	World Ocean Atlas 2018 (annual mean)
Satellite data	AVISO	CMEMS
L_D	first baroclinic deformation radius	$c_1/\sqrt{f^2+2c_1\beta}$, with c_1 = first surface mode gravity wave phase speed
$\mathcal{K}_0$	$\frac{\Gamma}{f}\left(\overline{M'M'}\right)^{1/2}$, with M = geostrophic streamfunction	$\Gamma u_{\text{rms}} L_{\text{mix}}$, with u_{rms} from surface EKE; $L_{\text{mix}} = L_D$
Γ	0.35	0.35
c_w	$\left(\overline{u}^{zt} - \beta L_D^2, \overline{v}^{zt}\right)$, with $\cdot^{zt}$ meaning averaged over time and depth	$\left(\overline{u}^{zt} - \beta L_D^2, \overline{v}^{zt}\right)$, with $\cdot^{zt}$ meaning averaged over time and depth
k	$2\pi/L_{\text{eddy}}$, with $L_{\text{eddy}} = 2.5L_D$	$2\pi/L_D$
γ^{-1}	4 days	1.68 days

Table 2. Properties, data sources, parameter values and expressions used for the diffusivity calculations by Chapman and Sallée (2017) and Groeskamp et al. (2020). Here, f is the Coriolis parameter and $\beta = df/dy$ is its latitudinal gradient.

the use of the SR1b data to derive a cross-stream coordinate for the mooring. Figure 4 illustrates how the cross-stream distance Y is computed for each measured profile, for both the section and the mooring data.

The transformation from temporal to spatial cross-stream coordinates in the data from the mooring thus requires a spatial data set that has sampled a cross-stream transect in the region of the mooring. If no hydrographic section data are available in the vicinity of a particular mooring, reanalysis products or climatologies could be used. We test this for the Argo, GLORYS and SOSE data (Table 1). Within each data set, the resulting spline fit is insensitive to the selected time period (Appendix A). For each of the three data sets, we interpolate the data to 30 locations along the SR1b line, and use the monthly profiles at these locations to fit the relation between Y and ϕ_{500}^{1500}.

The resulting ϕ-Y spline fits are shown in Figure 2b, together with the SR1b ϕ-Y spline fit. A smoothing factor of 0.85 is used for all data sets (see NG11 for a discussion about the choice of smoothing parameter). For the range of ϕ_{500}^{1500} spanned by the mooring (approximately 5.5–8.5 m^2s^{-2}), the Argo fit is the most similar to the SR1b fit. The GLORYS and SOSE fits follow each other closely in that range and are shifted southward compared to the other fits. For smaller values of ϕ_{500}^{1500}, the SOSE fit deviates substantially from the other fits, but this part is not relevant for the mooring data.

Importantly, the different data sets all show different characteristics around frontal jets in Drake Passage: the Polar Front (PF) and Sub-Antarctic Front (SAF). We define the locations of these fronts based on their value of ϕ_{500}^{1500}, following the definition from Naveira Garabato et al. (2009); the PF is at $\phi_{500}^{1500} = 0.55g$ and the SAF is at $\phi_{500}^{1500} = 0.7g$, with $g = 9.8\ \text{m}^2\text{s}^{-2}$ the gravitational acceleration. In the Argo, GLORYS and SOSE data, both the PF and the SAF are further south than in the

https://doi.org/10.5194/egusphere-2026-2566
Preprint. Discussion started: 8 May 2026

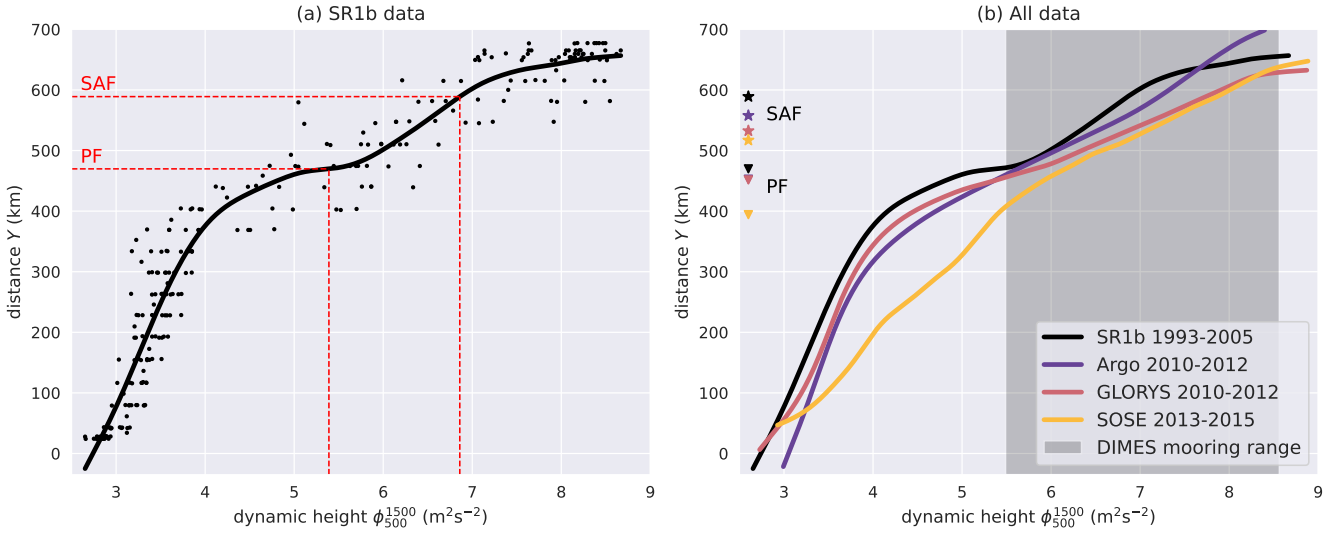

Figure 2. Spline fit for distance from the southernmost SR1b station location as a function of dynamic height ϕ_{500}^{1500}. (a) Measured data points together with spline fit for the SR1b data. The locations of the Polar Front (PF) and Sub-Antarctic Front (SAF) are indicated, based on the definition from Naveira Garabato et al. (2009). (b) Spline fits for the SR1b, Argo, GLORYS and SOSE data. The shaded area indicates the range covered by the mooring data. Along the vertical axis, the coloured triangles indicate the cross-stream locations of the PF, and the coloured stars indicate the locations of the SAF for each data set, again using the definition from Naveira Garabato et al. (2009).

SR1b data. Furthermore, the SR1b data shows relatively strong increases in ϕ_{500}^{1500} over short distances around the fronts; the other data sets show less strong increases. It may be that the coarser effective resolution of the Argo, GLORYS and SOSE data is missing parts of the eddy dynamics and thus fails to fully capture the structure of the fronts. In our analyses, we will try all spline fits shown in Figure 2b for deriving a cross-stream coordinate for the mooring data.

4.2 Temperature properties on neutral surfaces

Once we have computed the cross-stream position Y, we can study temperature properties as a function of Y and neutral density. Following NG11, we sort the temperature data into neutral density bins and then fit a spline relating Y to Θ on every neutral surface, using a smoothing factor of 10^{-14}. This spline denotes the large scale $\overline{\Theta}(Y)$. An important note is that the section samples a much larger range of ϕ_{500}^{1500} values than the mooring (Figure 2). This can affect the spline fits on neutral surfaces. To have good comparison between the section and mooring data, we remove all section profiles with a lower ϕ_{500}^{1500} value than the minimal value sampled by the mooring. We will discuss the impact of removing these section profiles in Section 5.1.

We use density bins with a spacing of 0.02 kg m^{-3}. This is the same resolution as was used by NG11 and gives a sufficient number of measurements to have robust spline fits for almost every density level. Again, to compare the section and mooring data, we consider only density levels that are covered by the mooring: between 27.14 kg m^{-3} and 28.20 kg m^{-3}. For the

https://doi.org/10.5194/egusphere-2026-2566
Preprint. Discussion started: 8 May 2026

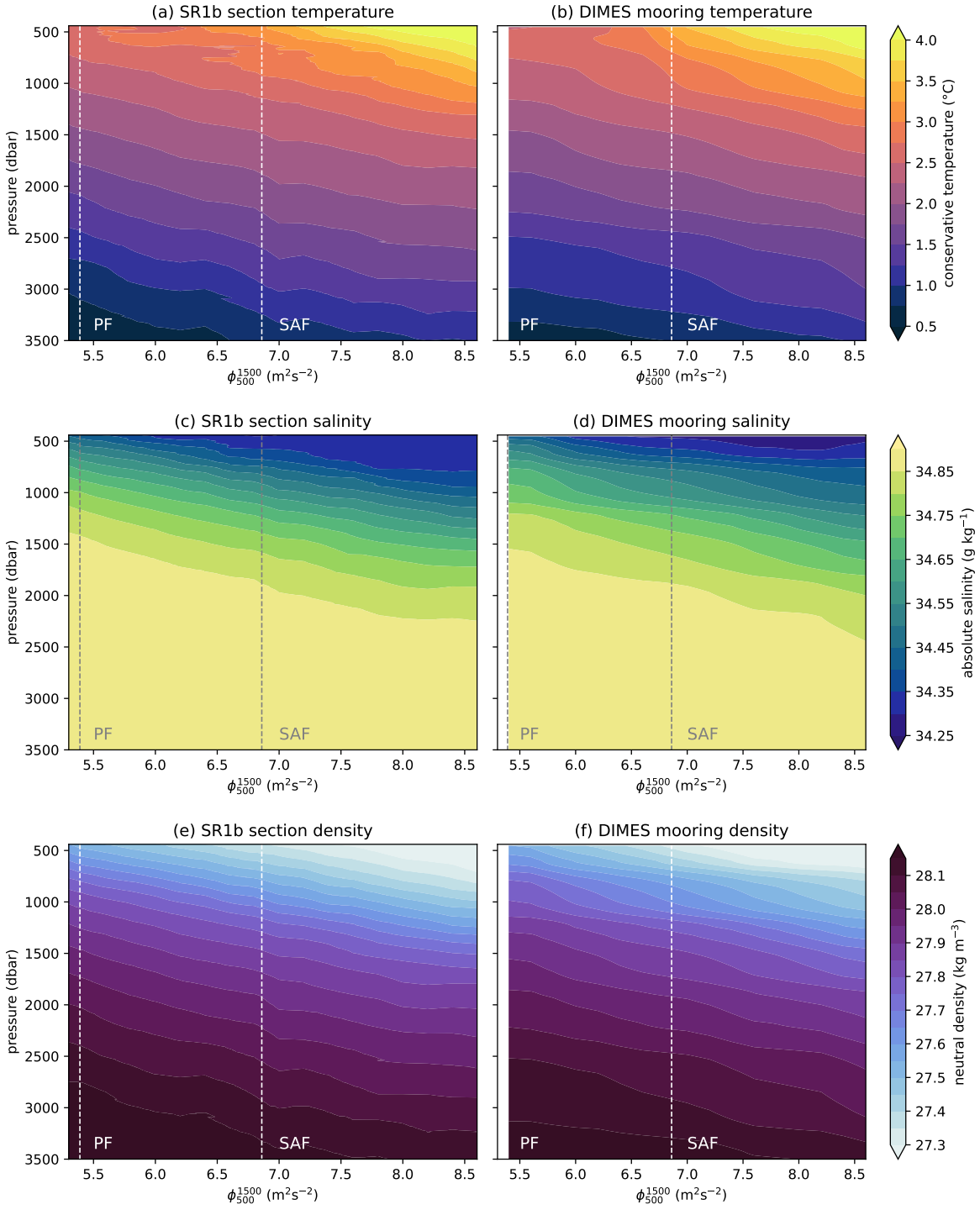

Figure 3. Running averages of conservative temperature, absolute salinity and neutral density profiles as a function of dynamic height ϕ_{500}^{1500} for the SR1b section data (left column) and the DIMES mooring data (right column). Locations of the Polar Front (PF) and Sub-Antarctic Front (SAF) are indicated, based on the definition from Naveira Garabato et al. (2009).

https://doi.org/10.5194/egusphere-2026-2566
Preprint. Discussion started: 8 May 2026

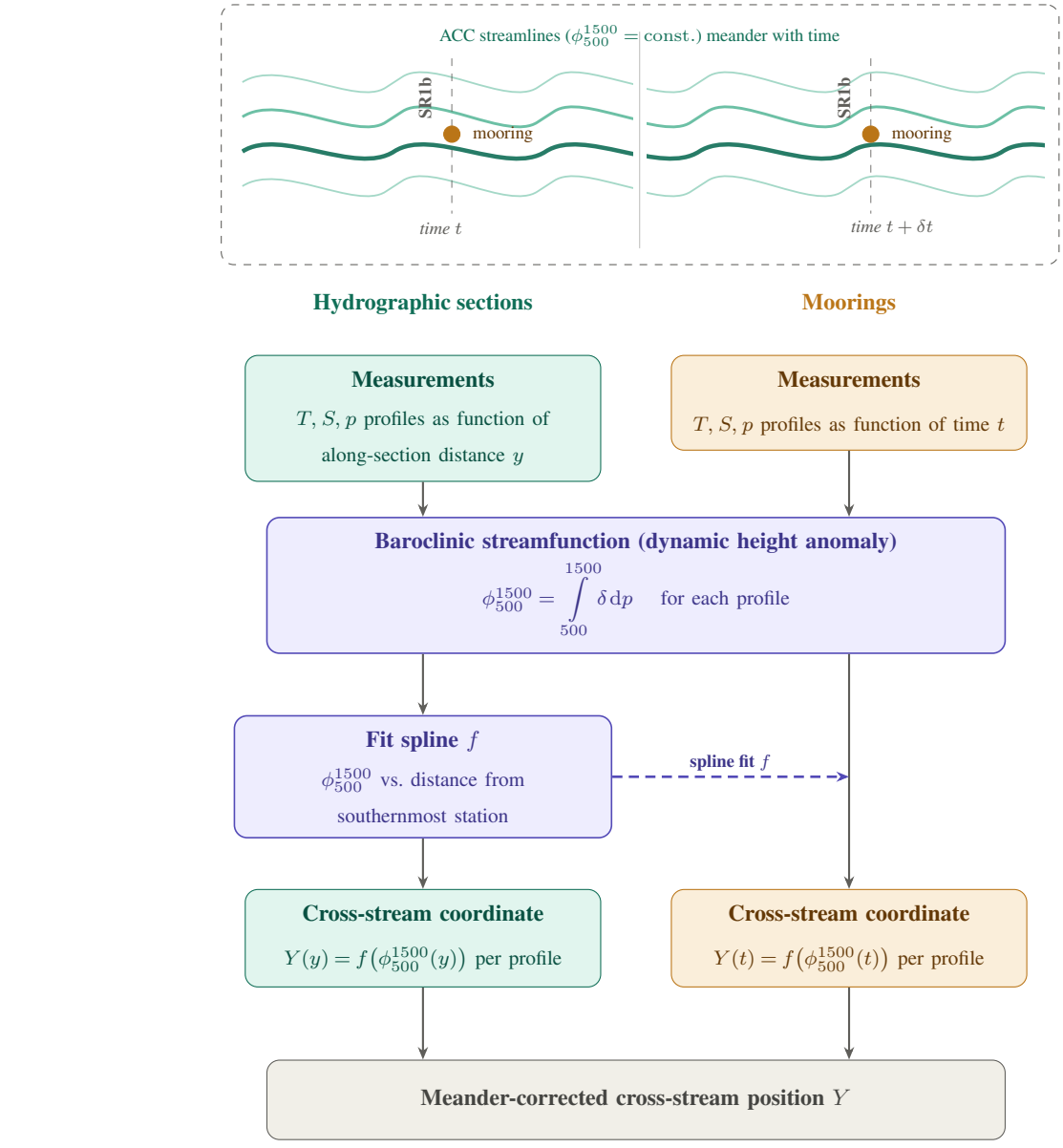

Figure 4. Schematic illustrating the transformation to the meander-corrected cross-stream position Y for both the hydrographic section data and the mooring data.

section data, each of these density bins contains at least 43 data points, with most density bins having between 80 and 100 data points. For the mooring data, the three lightest density bins contain less than 40 data points, but the other bins have many more points: most are even sampled by all 438 mooring profiles.

https://doi.org/10.5194/egusphere-2026-2566
Preprint. Discussion started: 8 May 2026

The rms temperature Θ_{rms} is then computed as the standard deviation of $\Theta - \overline{\Theta}(Y)$ for all measurements within a window $Y \pm \Delta Y$. We use a running window in Y with a grid spacing of 10 km and a window width of 40 km. It was discussed in NG11 that every calculation window should encompass at least 5–10 measurements for the calculation to converge, translating into window widths of 30–150 km. With our chosen grid spacing, for both the section and the mooring there are at most two calculation windows with less than 5 measurements. As most other windows have more than 10 measurements (in case of the moorings sometimes even more than 100), we deem this sufficiently robust. Indeed, for other window widths between 30 km and 150 km, the resulting eddy diffusivity distributions all show the same patterns (not shown).

Despite the fitted natural splines being smooth and differentiable, they are not necessarily monotonic. As a result, there might be local minima or maxima, leading to a vanishing gradient problem for $\partial_n \overline{\Theta}/\partial Y$ in equation (3). Consequently, the estimation of L_{mix}, and thereby $\mathcal{K}$, may reach unrealistically high values. To combat this, we impose an empirically chosen minimum value for the gradient $\partial_n \overline{\Theta}/\partial Y$ of 10^{-7} °C m^{-1}. Here the gradient should become indistinguishable from zero (Groeskamp et al., 2019).

NG11 showed all their resulting distributions as a function of Y and γ^n. We transform these to more intuitive coordinates: latitude along the section and depth. To transform from γ^n to depth, we also sort the measured depth (pressure) data into neutral density bins, and use those values to interpolate the hydrographic data back to depth levels with a vertical resolution of 68 m. During this interpolation step, values of the neutral gradients higher than the empirically chosen minimum value can occur. However, the cut-off values of the gradients are still used in the computation of the mixing length, which is done on the γ^n grid before interpolation. The cut-off value is again imposed on the interpolated neutral gradients.

4.3 Eddy velocity scale

In the computation of the cross-stream eddy velocity scale U_e (Equation 1), the mooring presents an advantage over the hydrographic sections: the mooring measures flow velocities. This is not the case for the hydrographic sections, so instead, NG11 derived the eddy velocity scale from altimetry data. We will not repeat their calculation here, and instead focus on the mooring velocity data. We compute U_e as follows. First we interpolate the u and v data to neutral surfaces, as we do for Θ and S_A. Per neutral surface, for each Y we compute the time-mean horizontal velocity vector $\overline{\mathbf{u}} = (\overline{u}, \overline{v})$ within a window $Y \pm \Delta Y$. The cross-stream direction is represented by $\hat{\mathbf{n}} = (-\overline{v}, \overline{u})/\sqrt{\overline{u}^2 + \overline{v}^2}$, the unit vector perpendicular to $\overline{\mathbf{u}}$. Then, $U_e(\gamma^n, Y)$ is computed as the standard deviation of the cross-stream velocity $\mathbf{u} \cdot \hat{\mathbf{n}}$ for all velocity measurements within the window $Y \pm \Delta Y$. In other words, U_e is the deviation of the mean cross-stream velocity, representative of the cross-stream eddy velocity.

We now have all the ingredients to compute eddy diffusivity for the mooring data; using dynamic height, we compute a cross-stream coordinate for each mooring profile, and compute cross-stream temperature and velocity properties on neutral surfaces. With these properties we can compute the mixing length using (3) and the eddy diffusivity with (1).

https://doi.org/10.5194/egusphere-2026-2566
Preprint. Discussion started: 8 May 2026

5 Results

5.1 Mean temperature field

The distributions of $\overline{\Theta}$ are shown in Figure 5. Figure 5a shows the 1993–2005 SR1b data, restricted to the range of latitudes (equivalent to ϕ_{500}^{1500} values) and depths that are covered by the mooring data. The 2010–2012 mooring data is shown in Figure 5b–e, for the four different data sets used to transform the mooring profiles to spatial coordinates using the fit between Y and ϕ_{500}^{1500}. The distributions of $\overline{\Theta}$ from the section data and the mooring data are highly comparable. Importantly, both data sets capture the strong horizontal stratification at the SAF. The PF, on the other hand, is not well captured in either data set. The choice of data set used to transform the mooring profiles to cross-stream coordinates impacts the distribution of the mooring data: it determines the range of cross-stream coordinates that is sampled as well as the positions of the profiles relative to each other, i.e. how much the data is 'stretched' or 'compressed' in the Y-direction. The locations of fronts are thus also moved for the different data sets. From Figure 2 we already saw that the ϕ-Y fit of the Argo data is closest to that of the SR1b data. This is also visible in Figure 5: the SR1b and Argo ϕ-Y fits yield approximately the same latitudinal range and $\overline{\Theta}$ distributions for the mooring data. Therefore, to restrict the number of figures, we will from now on only consider the mooring data using the SR1b and Argo ϕ-Y fits. Figures showing the results using the GLORYS and SOSE ϕ-Y fits as well can be found in Appendix B.

As described in Section 4.2, for the SR1b section data, we considered only those profiles within the range of ϕ_{500}^{1500} values covered by the mooring when making the spline fit of Θ to Y on neutral surfaces. To assess the impact of this, we consider Figure 6. In Figure 6a, the $\overline{\Theta}$ is shown as calculated from the full SR1b section data, including all profiles, and showing the full domain covered by those profiles (it thus shows the same data as Figure 5a of NG11, just in a different coordinate system). A variety of Southern Ocean water masses can be recognised. There is a large body of Circumpolar Deep Water (CDW; $\overline{\Theta} \sim 1 - 3°$C), with warmer Antarctic Intermediate Water (AIW) and Sub-Antarctic Mode Water (SAMW; both $\overline{\Theta} > 3°$C) overlying the CDW. Towards the south of the SR1b section, a volume of colder Antarctic Bottom Water (AABW; $\overline{\Theta} < 1°$C) can be found. Furthermore, the Polar Front is clearly visible in the form of a strong horizontal temperature gradient. Zooming in on the part of the domain covered by the mooring, we still see this signature of the PF. However, if we consider the $\overline{\Theta}$ distribution produced from the SR1b data excluding profiles outside the mooring range (Figure 6c, the same as Figure 5a), this strong horizontal stratification is missing. Moreover, the vertical stratification at the PF is also reduced. Apart from these differences, Figures 6b and c look very similar; in particular, both capture the high horizontal stratification at the SAF. We can thus conclude that the range of latitudes (or ϕ_{500}^{1500} values) sampled by the mooring is not large enough to accurately capture the PF, but it is sufficient for the SAF. More data points further south are required to retrieve the PF signature in the isopycnal temperature properties.

https://doi.org/10.5194/egusphere-2026-2566
Preprint. Discussion started: 8 May 2026

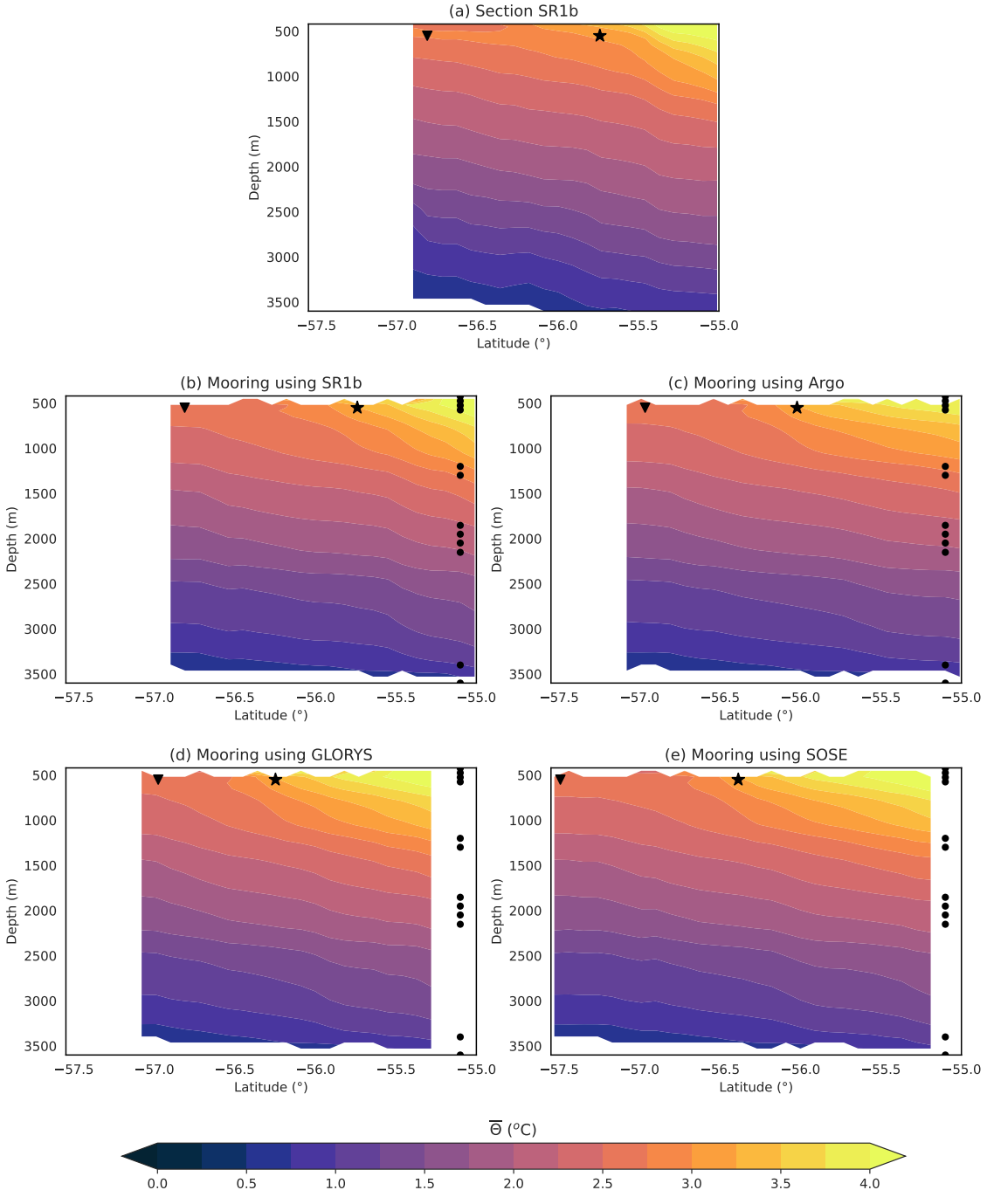

Figure 5. Distributions of $\overline{\Theta}$ as a function of latitude along the SR1b section and depth. (a) shows the SR1b section data; (b–e) show the mooring data, using different data sets to transform ϕ_{500}^{1500} to a cross-stream coordinate: the SR1b section data (b), Argo data (c), GLORYS data (d) and SOSE data (e). The Polar Front is indicated with a triangle and the Sub-Antarctic Front is indicated with a star; their locations are based on the definition from Naveira Garabato et al. (2009). The black dots indicate the instrument depths of the mooring.

https://doi.org/10.5194/egusphere-2026-2566
Preprint. Discussion started: 8 May 2026

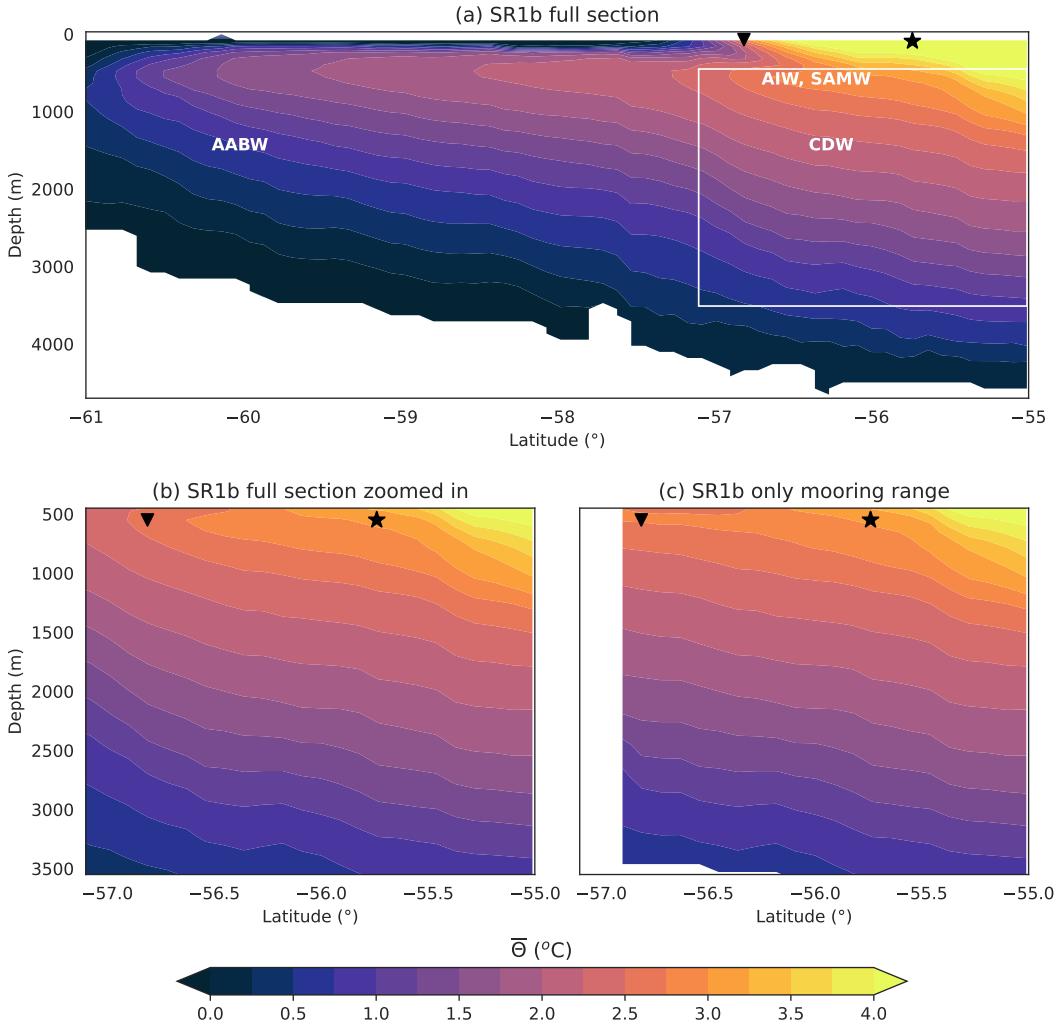

Figure 6. Distributions of $\overline{\Theta}$ as a function of latitude along the SR1b section and depth. (a) shows the full SR1b section; here all SR1b profiles were taken into account when making the spline fit of Θ to Y on neutral surfaces. (b) shows a zoomed-in part of (a), corresponding to the part of the domain covered by the mooring (indicated by the rectangle in (a)). (c) shows that same part, but here the spline fits of Θ to Y on neutral surfaces were made using only those SR1b profiles with a value of ϕ_{500}^{1500} higher than the minimum value sampled by the mooring. The Polar Front is indicated with a triangle and the Sub-Antarctic Front is indicated with a star; their locations are based on the definition from Naveira Garabato et al. (2009). In (a), the different water masses are also indicated.

https://doi.org/10.5194/egusphere-2026-2566
Preprint. Discussion started: 8 May 2026

5.2 Cross-stream isopycnal gradients and rms temperature

Figure 7a–c shows the absolute value of the cross-stream isopycnal temperature gradient, $|\partial_n \overline{\Theta}/\partial Y|$. There are some important differences between the section data and the mooring data. The section data shows reduced gradients near the surface at the PF and the SAF. The mooring data also has weak gradients at the PF, but higher gradients at the SAF. Furthermore, in the interior, in the SR1b data the gradients become very weak, and are largely at the imposed cut-off value of 10^{-7} °C m^{-1}. By contrast, the gradients from the mooring data are overall higher, with local maxima between 2000–2500 m.

The distributions of the rms temperature fluctuations along isopycnals are shown in Figure 7d–f. The patterns of the rms fluctuations broadly follow those of the isopycnal gradients. The section and mooring data give quite good agreement, particularly at the shallowest levels (500–1000 m), although the section-based values are somewhat higher. At deeper levels, Θ_{rms} is generally lower for the mooring than for the section, especially in the southern part of the domain.

5.3 Mixing length, eddy velocity scale and eddy diffusivity

From the hydrographic properties presented in the previous sections, we can derive the mixing length from equation (3). The result is shown in Figure 7g–i. Calculated based on the contributions from the isopycnal gradients and rms fluctuations, we indeed see that spatial patterns reminiscent of both emerge. The mixing length distribution shows strong spatial variations, spanning at least two orders of magnitude. Overall the mixing length is lower in the mooring data than in the section data. Both the section and the mooring data show an area of elevated L_{mix} near the surface in between the PF and SAF; in the section data, this area even covers the PF. The section has a second area of elevated L_{mix} to the north and deeper than the first; this area is not seen in the mooring data. Features that are present in the mooring data but absent in the section data are bands of elevated L_{mix} around 2000 m and around 3000 m depth, matching the regions of very low temperature gradients.

We can combine the mixing length with the cross-stream eddy velocity scale U_e to compute eddy diffusivities. The distribution of U_e is shown in Figure 8. As the hydrographic section data does not contain velocity measurements, only the mooring data are considered here. The SR1b and Argo ϕ-Y fits yield largely the same structure, with high cross-stream eddy velocities in the north and weaker velocities in the south, though with a local maximum near the PF. All along the section, U_e monotonically decreases with depth, reflecting the equivalent barotropic structure of the ACC. Note that the frontal regions do not correspond to the regions with the highest U_e.

From L_{mix} and U_e, we compute the cross-stream eddy diffusivity $\mathcal{K}$ for the mooring data, shown in Figure 9a–b. For the calculation we use equation (1) with the mixing efficiency Γ set to 0.35 (Klocker and Abernathey, 2014). Clearly, the distribution of $\mathcal{K}$ is dominated by L_{mix}, while U_e has only a limited impact. The eddy diffusivity shows the same spatial patterns as L_{mix}, with high values at the base of the mixed layer between the PF and the SAF, and high values around 2000 m and, to a lesser extent, around 3000 m depth. The SR1b and Argo ϕ-Y fits produce largely the same distributions, with the main difference that the Argo fit gives much higher diffusivities in the north.

https://doi.org/10.5194/egusphere-2026-2566
Preprint. Discussion started: 8 May 2026

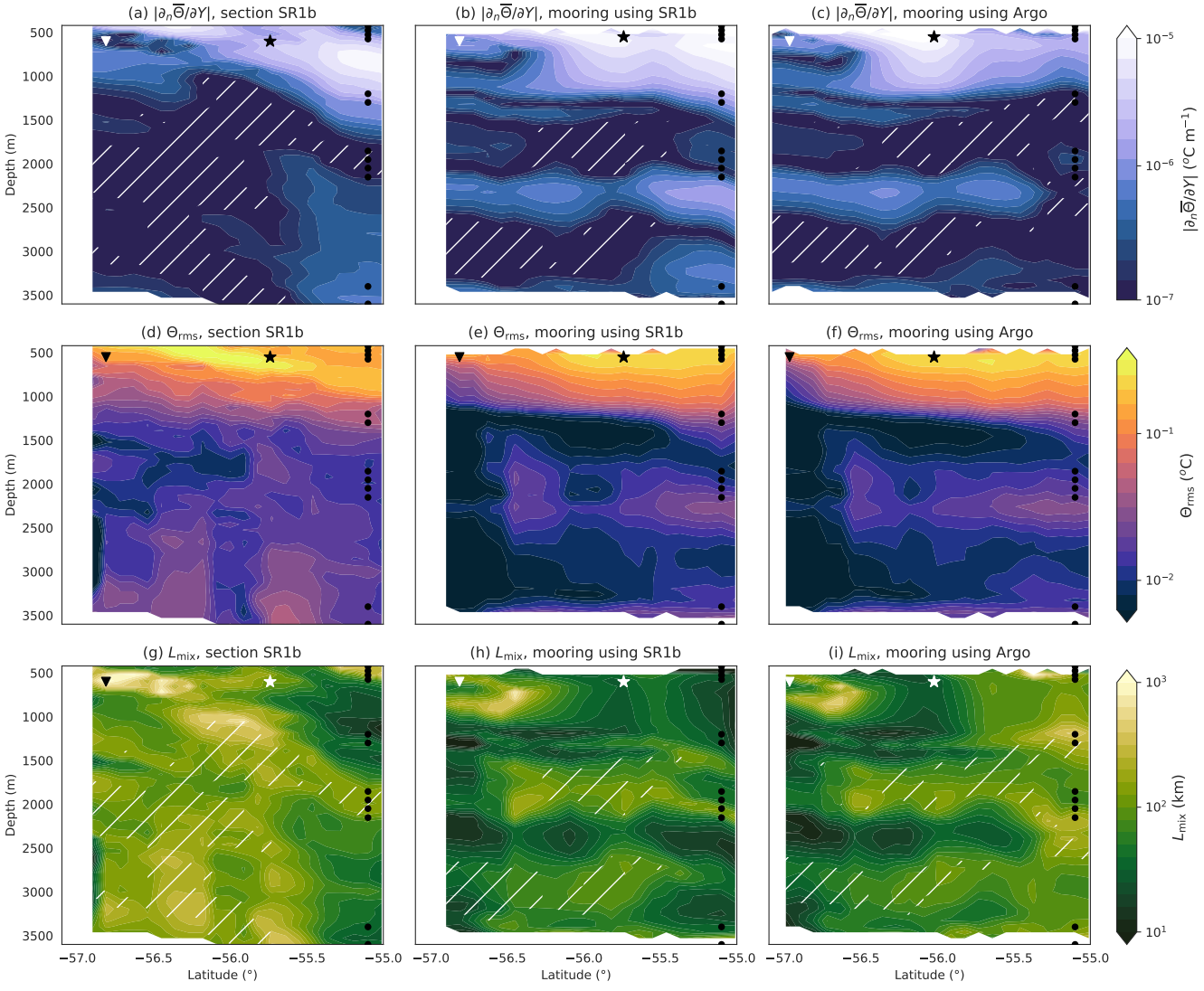

Figure 7. Distributions of (a–c) $|\partial_n \overline{\Theta}/\partial Y|$, (d–f) Θ_{rms} and (g–i) the mixing length as a function of latitude along the SR1b section and depth. The first column shows the SR1b section data; the second column shows the mooring data using SR1b data to transform transform ϕ_{500}^{1500} to a cross-stream coordinate; the third column shows the mooring data using Argo data for the transformation. The Polar Front is indicated with a triangle and the Sub-Antarctic Front is indicated with a star; their locations are based on the definition from Naveira Garabato et al. (2009). The black dots indicate the instrument depths of the mooring. In (a–c) and (g–i), the hatched regions are where $|\partial_n \overline{\Theta}/\partial Y|$ has been set to the minimum value of 10^{-7} °C m^{-1}.

https://doi.org/10.5194/egusphere-2026-2566
Preprint. Discussion started: 8 May 2026

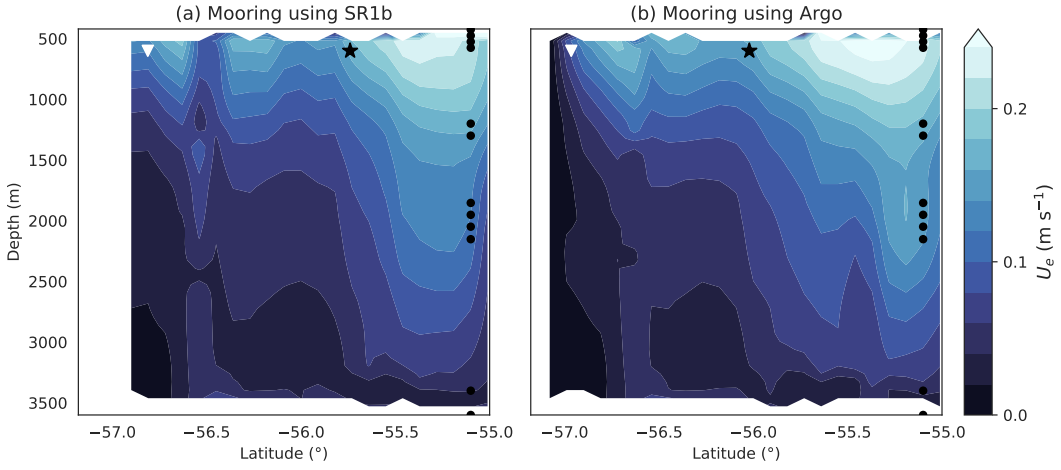

Figure 8. Distributions of the cross-stream eddy velocity scale as a function of latitude along the SR1b section and depth. (a) shows the mooring data using SR1b data to transform transform ϕ_{500}^{1500} to a cross-stream coordinate; (b) shows the mooring data using Argo data for the transformation. The Polar Front is indicated with a triangle and the Sub-Antarctic Front is indicated with a star; their locations are based on the definition from Naveira Garabato et al. (2009). The black dots indicate the instrument depths of the mooring.

5.4 Comparison with other eddy diffusivity data sets

Our eddy diffusivity estimate is based on isopycnal gradients and fluctuations of temperature. We can thus consider it as a hydrographic or thermodynamic approach to computing eddy diffusivity. However, there are other methods of deriving eddy diffusivity based on kinematic or dynamical approaches, such as equation (5) that was used by CS17 and G20 (Section 3.4). We compare the data of CS17 and G20 to ours by interpolating their diffusivity estimates to the coordinates along the SR1b section. The results are shown in Figures 9c–d. Note that CS17 has no data below depths of 1975 m, while G20 has no data for the northern end of the section in the depth range considered here.

The CS17 and G20 diffusivities differ from the mooring-derived diffusivities in order of magnitude, with the mooring-derived diffusivities generally being higher. However, the CS17 and G20 diffusivities also differ strongly from each other, with the G20 diffusivities being roughly a factor 10 smaller. In the CS17 data, two areas of increased diffusivity show up near the surface, which roughly correspond to the regions of high diffusivity found from the mooring data. By contrast, the G20 values are almost horizontally uniform. This is likely due to the low spatial resolution of the G20 data and the amount of smoothing for constructing the World Ocean Atlas data set it was based on; the SR1b section is distributed over only five of the grid cells in the G20 data set. The G20 data thus does not capture the frontal jets in the upper part of the water column. Considering the vertical structure, the CS17 diffusivity decreases with depth almost everywhere, reaching minimum values at its deepest levels close to 2000 m. By contrast, both the G20 data and the mooring data show increased diffusivities between 1500–2000 m.

https://doi.org/10.5194/egusphere-2026-2566
Preprint. Discussion started: 8 May 2026

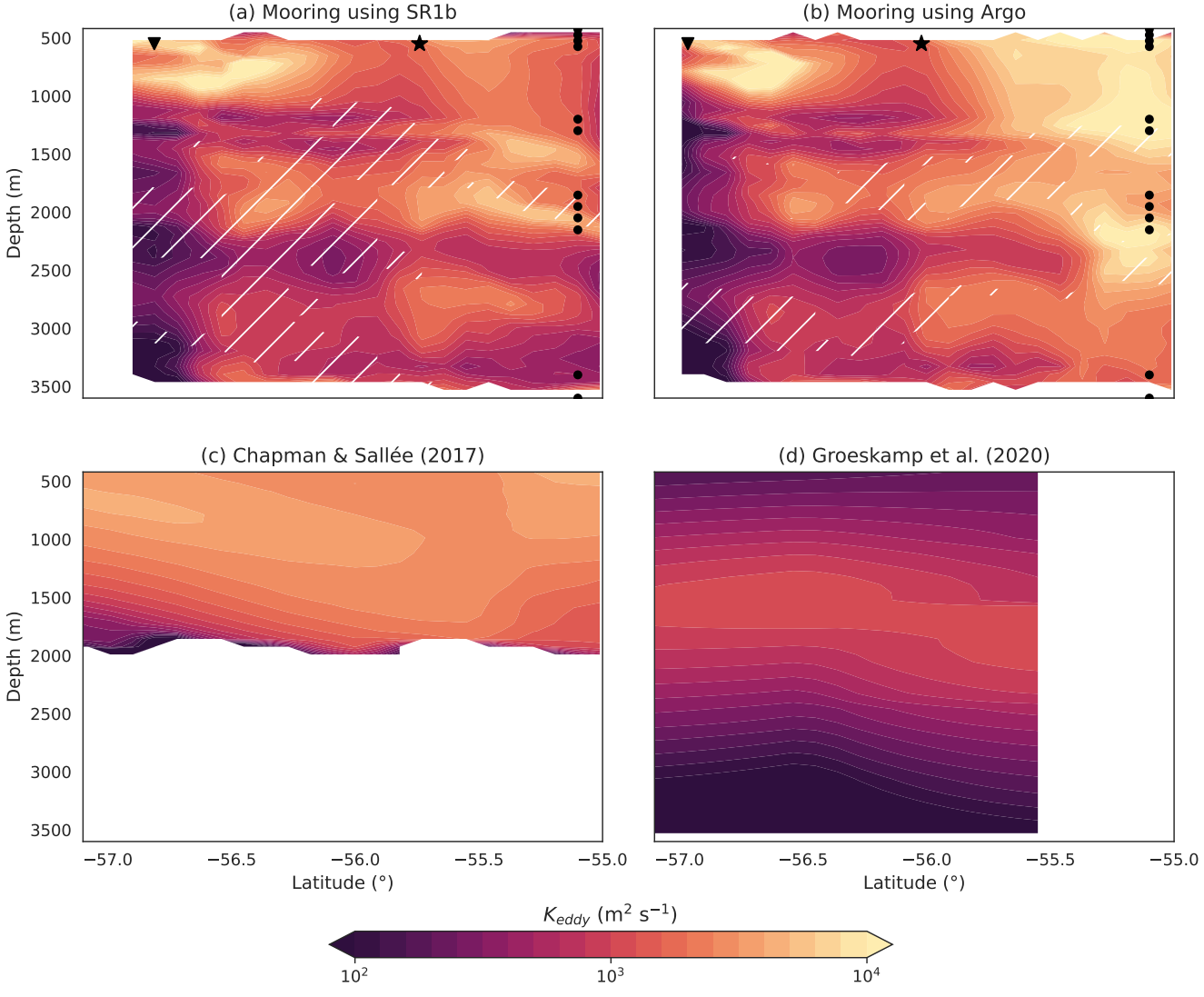

Figure 9. Distributions of the cross-stream eddy diffusivity as a function of latitude along the SR1b section and depth. (a) shows the mooring data using SR1b data to transform transform ϕ_{500}^{1500} to a cross-stream coordinate; (b) shows the mooring data using Argo data for the transformation; (c) shows the diffusivity from Chapman and Sallée (2017); (d) shows the diffusivity from Groeskamp et al. (2020). In (a) and (b), the Polar Front is indicated with a triangle and the Sub-Antarctic Front is indicated with a star; their locations are based on the definition from Naveira Garabato et al. (2009). The black dots indicate the instrument depths of the mooring. In (a) and (b), the hatched regions are where $|\partial_n \overline{\Theta}/\partial Y|$ has been set to the minimum value of 10^{-7} °C m^{-1}.

https://doi.org/10.5194/egusphere-2026-2566
Preprint. Discussion started: 8 May 2026

6 Discussion

6.1 Advantages, shortcomings and applicability of methodology

Our method uses dynamic height anomaly to transform the temporal coordinate of the mooring data to a spatial (cross-stream) coordinate. Comparison of the mooring-derived and section-derived distributions can give an idea of how this method performs in producing cross-stream distributions from mooring time series. The mooring-derived and section-derived cross-stream distributions of the mean temperature look very similar (Figure 5). The main difference is around the PF. The mooring completely misses the expected strong horizontal stratification here, but the section does not capture it accurately, either. This is due to the PF being at the edge of the range of Y-values that is considered for the spline fits of Θ to Y, while part of the dynamics around the PF comes from further south; if a larger southern portion of the section is taken into account for the spline fits, the PF signature does become visible (Figure 6). Next, looking at the distributions of the isopycnal temperature gradient (Figure 7a–c), we see that the SAF signature near the surface is captured better by the mooring than by the section data: the mooring shows a higher isopycnal gradient here. Another difference between the section and mooring is that the mooring has increased gradients between 2000–2500 m depth. Differences in the isopycnal gradients stem on one hand from differences in measurements from the section and the mooring, which may be due to the different time periods during which they were taken, as there is seasonal and interannual variability in hydrographic properties and locations of fronts (Naveira Garabato et al., 2009; Kim and Orsi, 2014; Giglio and Johnson, 2016; Freeman et al., 2016). On the other hand, numerical inaccuracies and sensitivity of the spline fits may play a role. Finally, the distributions of Θ_{rms} show good agreement between the section and mooring data, except for some deeper levels where the mooring gives much lower rms values (Figure 7d–f). The mooring generally has a lower spread between the data points.

An advantage of the mooring data is that it includes velocity measurements, such that we can derive a cross-stream eddy velocity scale. By contrast, when relying on hydrographic section data, other data sources and/or assumptions are required for deriving an eddy velocity scale; for example, NG11 used satellite altimetry products and calculated vertical profiles of velocity using geostrophic shear. When using mooring data, we can thus get an estimate of the eddy diffusivity based completely on measurements from the mooring (except for the transformation to cross-stream coordinates).

There are also some disadvantages of using mooring data over using section data, however. First, the mooring measurements have very low vertical resolution compared to the section data, with only 12 instrument depths. Here we interpolated the mooring data to a vertical resolution of 10 dbar before calculating the temperature and velocity properties on neutral surfaces, but it is possible that smaller-scale vertical variability is not accurately captured by the moorings, which could impact the obtained isopycnal temperature gradients and fluctuations. The effect of the vertical resolution can be tested by subsampling the section data to lower vertical resolution and then repeating all the calculations. The resulting distributions of the mixing length are shown in Figure 10. When the original data at 2 dbar resolution is downsampled to 100 or 150 dbar, the resulting L_{mix} distributions are largely unaffected, but at 200 dbar, clear differences start to show; most notably, the disappearance of the high L_{mix} area in the interfrontal region. This illustrates that the low vertical resolution of the moorings could be problematic. On the other hand, the interpolated mooring data produce largely the same distributions of mean temperature as the section

https://doi.org/10.5194/egusphere-2026-2566
Preprint. Discussion started: 8 May 2026

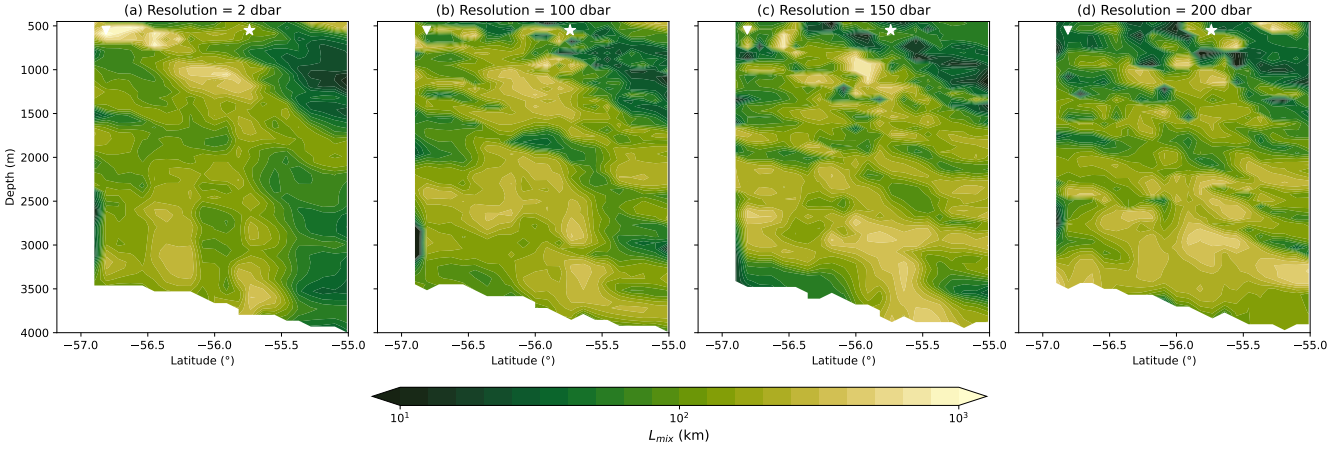

Figure 10. Distributions of the mixing length calculated from the SR1b section data. (a) shows the result of using the original data; (b–d) show the results of using the data downsampled to a lower vertical resolution. The Polar Front is indicated with a triangle and the Sub-Antarctic Front is indicated with a star; their locations are based on the definition from Naveira Garabato et al. (2009).

data (Figure 5), so interpolation can be helpful. Moreover, the interpolated mooring data accurately captures Θ_{rms} (Figure 7d–f), which represents the variability associated with isopycnal stirring. Jakes et al. (2025) showed that interleaving features in the ACC are of $\mathcal{O}(10\ \mathrm{m})$ thick, but the layers containing many interleaving features can be $\mathcal{O}(100\ \mathrm{m})$ thick; the mooring is thus still capturing the bulk of the interleaving features and representing the stirring signal well. Applying our method with interpolated mooring data is expected to work best in equivalent barotropic systems. Generally, a higher vertical resolution in moorings should improve the suitability of our method.

Further, the mooring only samples a range of ϕ_{500}^{1500} values corresponding to the northern end of the section, but doesn't capture the area south of the PF. The sampled range of ϕ_{500}^{1500} is of width comparable to the characteristic cross-stream scale of the large-scale background field, which is of $\mathcal{O}(100\ \mathrm{km})$. On the other hand, the mooring does have many more measurements within this range of ϕ_{500}^{1500}, as its high temporal resolution gets translated to a high spatial resolution. This could make the spline fits on neutral density surfaces more robust.

Finally, our method still depends on hydrographic section data to transform the mooring profiles to cross-stream coordinates. These may not be available at all locations and time periods, and are still costly and time-consuming to measure. As an alternative, we proposed to use readily available data sets and sample those along the section instead. We compared data from Argo and from the GLORYS and SOSE reanalyses. All three data sets yield ϕ-Y fits that are different from the SR1b section data; the PF and SAF are shifted southwards, and the strong increases in dynamic height around the fronts is absent. Apart from that, though, the data sets provide good smoothed alternatives for first order estimates. In the region studied here, the Argo data give the best correspondence with the SR1b section data. The main difference between the SR1b and Argo ϕ-Y fits in the resulting distributions from the moorings is that the Argo fit gives much higher eddy diffusivities at the northern end of the section.

https://doi.org/10.5194/egusphere-2026-2566
Preprint. Discussion started: 8 May 2026

That the readily available data sets yield comparable cross-stream distributions from the moorings as the SR1b data, inspires exploring the wider applicability of our methodology to other moorings. Some caution is required here, though. Firstly, the accuracy of different climatologies and reanalysis products may vary throughout the ocean, and may not be good alternatives to in-situ measurements everywhere. Secondly, the dynamic height anomaly at 500 dbar relative to 1500 dbar may not be a good representation of a cross-stream coordinate everywhere. In this study, the exact choice of pressure levels did not have a strong impact because the ACC is equivalent-barotropic. In other ocean regions, other pressure levels may be required, or a different variable altogether. This depends on the horizontal structure of the mean current, the vertical structure of the temperature field and the depth of the water column at the mooring locations.

6.2 Cross-stream isopycnal eddy diffusivity values derived from mooring data

Although we lack a 'ground truth' for the horizontal and vertical structure of eddy diffusivity in Drake Passage, we can still compare the mooring-derived diffusivity distributions with other methods and theories, to say something about how realistic our distributions are. One important feature of the mooring-derived diffusivities is the structure near the surface: the diffusivity is reduced around the SAF (Figure 9). In the context of mean flow suppression theory, we expect decreased diffusivities in regions with strong background currents, such as frontal jets. The mooring-derived diffusivity distributions support this hypothesis. Although we would expect the same to hold for the PF, recall that the mooring is located too far north to accurately represent the PF (Figures 5, 6, 7; Section 6.1).

Another key feature of the mooring data is the band of elevated diffusivities between 1500–2000 m depth. A similar mid-depth maximum in diffusivity is found in the data from G20. The existence of this mid-depth maximum in the ACC, the 'steering level' where mean flow and eddy phase speeds are equal, is broadly supported by evidence from other theoretical and modelling studies, with depth estimates ranging from 1 to more than 2 km (Smith and Marshall, 2009; Abernathey et al., 2010; Vollmer and Eden, 2013; Tulloch et al., 2014; Griesel et al., 2015). In our method, the mid-depth maximum is the result of weak neutral gradients (equation 3 and Figure 7). The fact that our hydrographic approach is able to capture the mid-depth maximum which is usually defined using kinematic arguments, is therefore a positive feature of our method. Importantly, the mid-depth maximum in the mixing length is not captured by the SR1b section data, but it is captured by the mooring data using either the SR1b or Argo ϕ-Y fit (Figure 7g–i).

It is also relevant to consider the order of magnitude of our diffusivities. In the aforementioned areas with increased diffusivities both near the surface and at mid-depth, diffusivity values become as large as 10^4 m^2/s. These values are unrealistically high. Note that the section data yielded even larger diffusivity values in NG11 (their Figure 5g). A possible problem is the computation of the neutral gradients, which become very small here. We tried to remedy this by imposing a cut-off value for the gradients, but they still become small enough to be practically indistinguishable from zero. Another possible source of the high diffusivity values is that the assumptions behind equation (3) for the mixing length break down in these regions: temperature and salinity fluctuations could be transported here from upstream, rather than generated locally. For example, the occasional injection of a different CDW type from a boundary current entering northern Drake Passage from the subtropical Pacific could be to blame (Brearley et al., 2014). Outside the regions with very high diffusivities, though, the diffusivity values

https://doi.org/10.5194/egusphere-2026-2566
Preprint. Discussion started: 8 May 2026

are in the range of $10^2 - 10^3$ m^2/s, which is in line with both CS17 and estimates from other studies (Naveira Garabato et al., 2007; LaCasce et al., 2014; Roach et al., 2016). Our diffusivities are still generally higher than those of CS17 and G20. The discrepancy may be caused by topographic effects. Topography is known to impact eddy diffusivities (Sterl et al., 2024; Deng and Wang, 2024; Dettling et al., 2025). Roach et al. (2016) show that mean flow suppression theory, which both CS17 and G20 based their calculations on, underestimate the observed particle-based diffusivities in parts of the Southern Ocean with strong topographic features. They suggest this is because mean flow speeds are elevated here, as the ACC streamlines are squeezed together while traversing over the topographic features. The topographic slope at the DIMES mooring location is indeed quite steep – approximately 2×10^{-2} m/m, as computed from the GLORYS bathymetry; hence it is plausible that the topography affects the dynamics. Finally, note that the magnitudes and distributions of CS17 and G20 also don't agree with each other, even though both calculations are based on mean flow suppression theory. A relevant difference is that the G20 values were calibrated based on other observational values from, among others, the DIMES region, and are thus closer to other observations than the CS17 values (see Figure 1b of G20). Furthermore, differences between the mooring data, CS17 and G20 values may be caused by differences in time scales. While the mooring-based diffusivities are based on a short time period of just over a year, the CS17 calculation is based on Argo data spanning almost a decade, and the G20 values are calculated from long time averages (World Ocean Atlas).

7 Conclusions

We presented a method to derive distributions of cross-stream isopycnal eddy diffusivities from mooring data, based on computing a mixing length from isopycnal temperature gradients and rms fluctuations. Applied to a mooring in Drake Passage, our method revealed eddy diffusivity distributions that captured some key features supported by other studies: decreased diffusivities at the base of the mixed layer at the SAF frontal jet and increased diffusivities at mid-depths. Although the values are sometimes unrealistically high, the qualitative patterns found from the mooring data are consistent with other work.

A key ingredient of the method is transforming the temporal variability measured by the moorings to spatial variability. Calculating the dynamic height ϕ_{500}^{1500} and using a fitted spline relation (ϕ_{500}^{1500} to Y) from hydrographic section data, we transform the temporal coordinates from the mooring data to spatial coordinates. Spatial distributions of thermohaline properties are thus not measured directly, but inferred from the motion of the ACC across the mooring. As an alternative to hydrographic section data, readily available data sets such as climatologies or reanalyses can be used for the spline fit between ϕ_{500}^{1500} to Y. This means that our method holds potential even for moorings with no hydrographic section data available, or for future mooring studies which won't require hydrographic transects. This has considerable implications for the versatility of data obtained from moorings. Even with a relatively low vertical resolution, it is possible to characterise the cross-stream and vertical structure of eddy stirring in the ACC using a single mooring, with quite fine detail because the current meanders back and forth across the mooring. We expect this method to work well in other equivalent barotropic currents, and recommend a higher vertical resolution wherever possible.

https://doi.org/10.5194/egusphere-2026-2566
Preprint. Discussion started: 8 May 2026

The results presented here thus offer encouragement to apply the method to other moorings throughout the ocean, which could give relevant insights into horizontal and vertical structures of eddy diffusivity. This is important as eddy diffusivity distributions throughout the ocean are still highly uncertain. The lack of consistency between different diffusivity data sets, such as the CS17 and G20 data discussed here, highlights the need for further research. The method discussed in this paper, deriving eddy diffusivities from mooring data, can be a valuable addition to the toolbox for estimating isopycnal eddy diffusivities.

Code and data availability. The SR1b hydrographic section data is available at https://noc.ac.uk/projects/drake-passage. The DIMES mooring data is available at https://www.bodc.ac.uk/data/bodc_database/.

The Roemmich-Gilson Argo climatology was downloaded from https://sio-argo.ucsd.edu/RG_Climatology.html. These data were collected and made freely available by the International Argo Program and the national programs that contribute to it (http://www.argo.ucsd.edu, http://argo.jcommops.org). The Argo Program is part of the Global Ocean Observing System. http://doi.org/10.17882/42182

The GLORYS12V1 data was downloaded from https://doi.org/10.48670/moi-00021.

The SOSE data was downloaded from https://sose.ucsd.edu/SO6/ITER156/MONTHLY/DP/.

The diffusivity data from Chapman and Sallée (2017) was downloaded from https://datadryad.org/dataset/doi:10.5061/dryad.55bp8#citations.

The diffusivity data from Groeskamp et al. (2020) was downloaded from https://figshare.com/articles/dataset/Groeskamp_et_al_2020_-_mixing_diffusivities/12554555.

The code used in this study can be found at https://github.com/MiriamSterl/SouthernOceanMooringDiffusivity. The exact data files used and calculated in this work can be shared upon request.

Appendix A: Sensitivity of ϕ-Y spline fits to different time periods

Figure A1 shows the spline fits between Y and ϕ_{500}^{1500} for the Argo, GLORYS and SOSE data for different time periods of each data set. For Argo and SOSE, we compare the full available range of the data with the subset of 3 years that are closest to the years of the DIMES mooring data. For GLORYS, we compare the period overlapping with the SR1b hydrographic section data with the period of the DIMES mooring data. We also check only the months November, December and January (the summer months during which the SR1b sections were taken). For all three data sets, the resulting spline fits are not significantly impacted by the choice of time period.

https://doi.org/10.5194/egusphere-2026-2566
Preprint. Discussion started: 8 May 2026

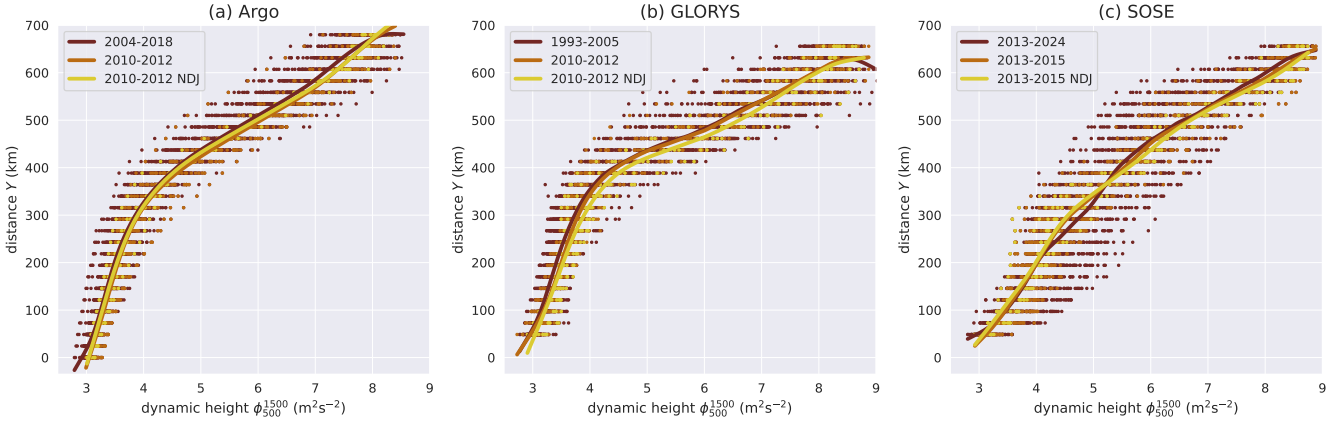

Figure A1. Spline fits for distance from the southernmost SR1b station location as a function of dynamic height ϕ_{500}^{1500}, for three different data sets and for three different time periods of each data set. The dots mark the individual data points.

https://doi.org/10.5194/egusphere-2026-2566
Preprint. Discussion started: 8 May 2026

Appendix B: Temperature properties for all data sets

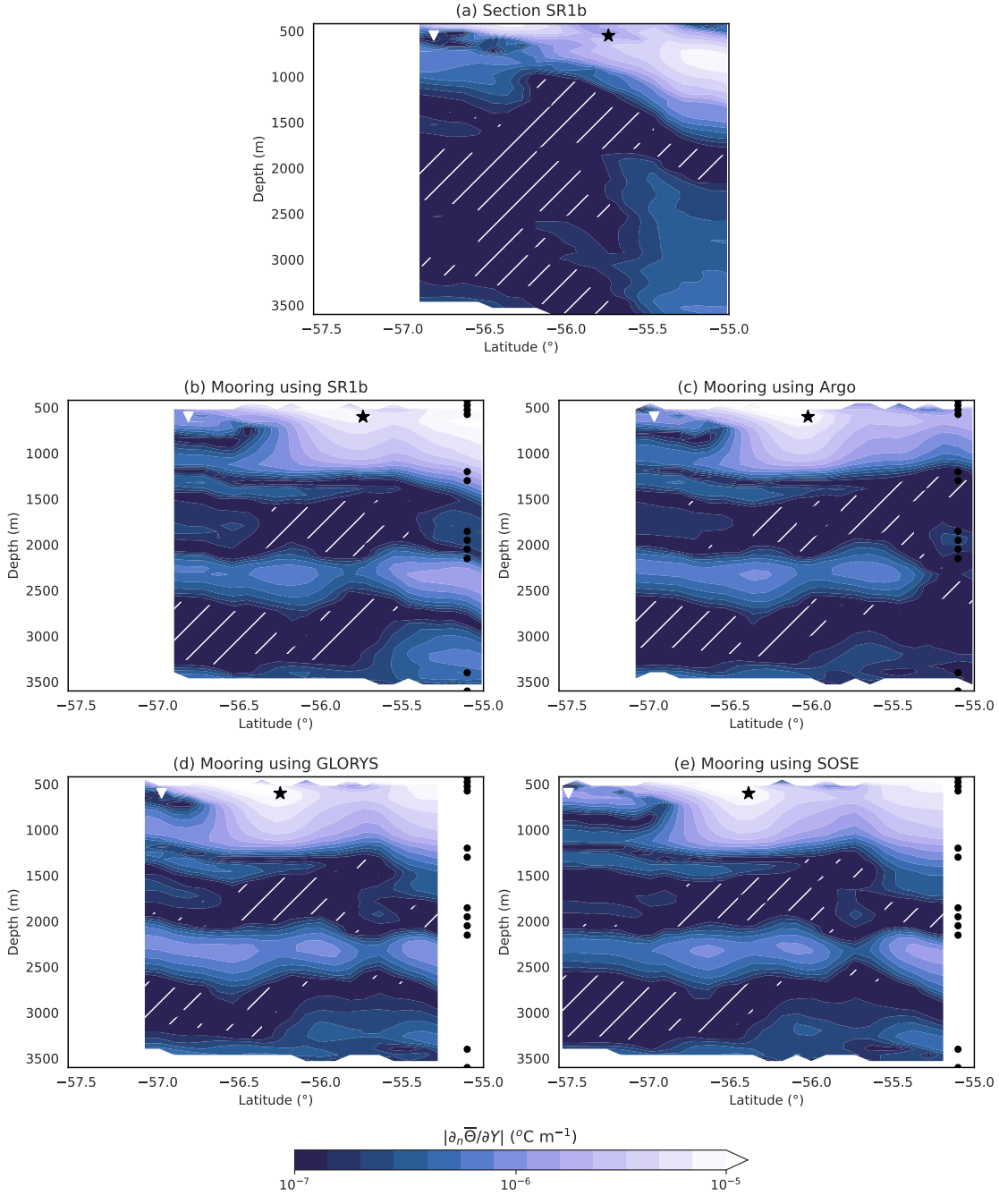

Figure B1. As Figure 5 but for $|\partial_n \overline{\Theta}/\partial Y|$.

https://doi.org/10.5194/egusphere-2026-2566
Preprint. Discussion started: 8 May 2026

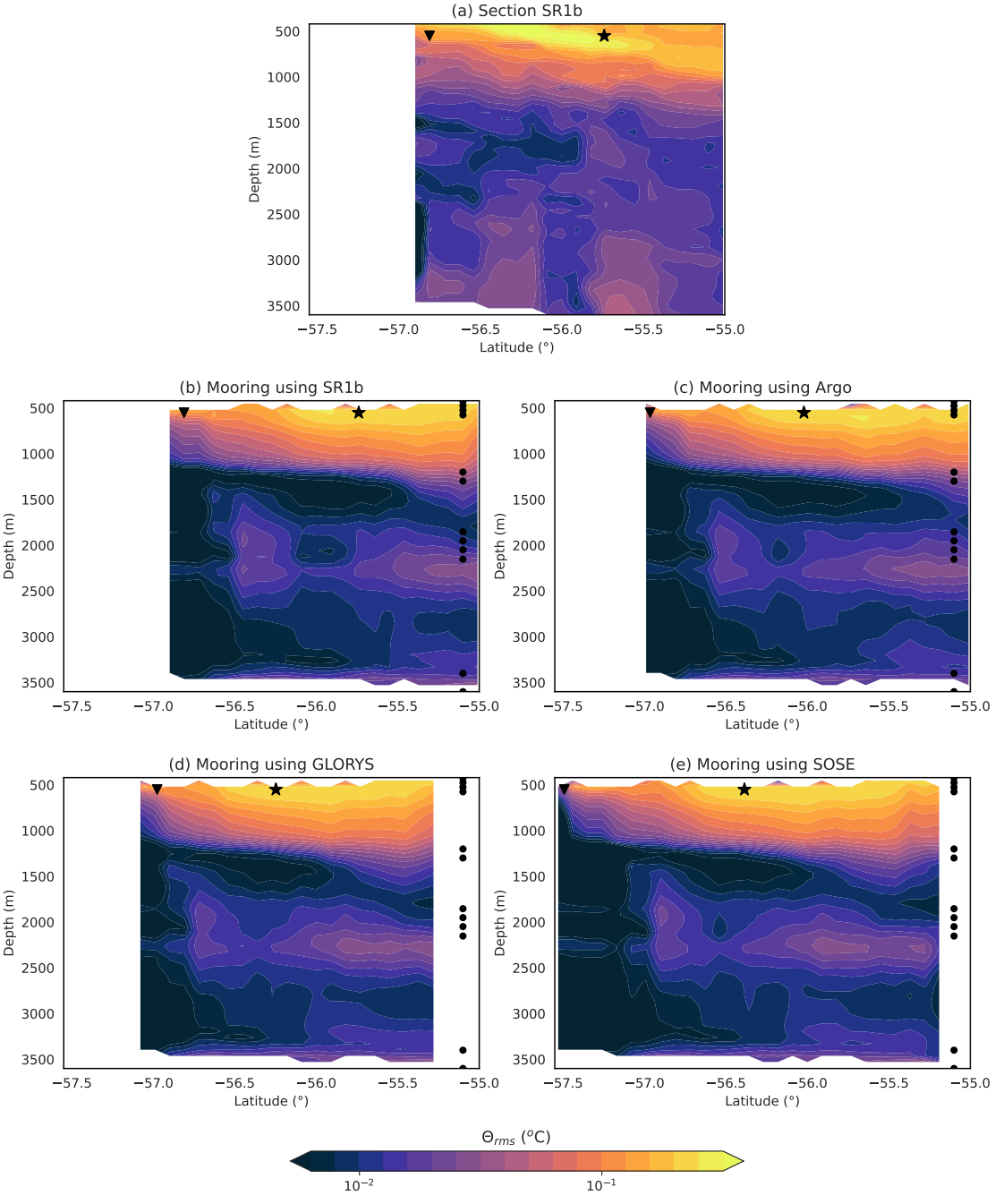

Figure B2. As Figure 5 but for Θ_{rms}.

https://doi.org/10.5194/egusphere-2026-2566
Preprint. Discussion started: 8 May 2026

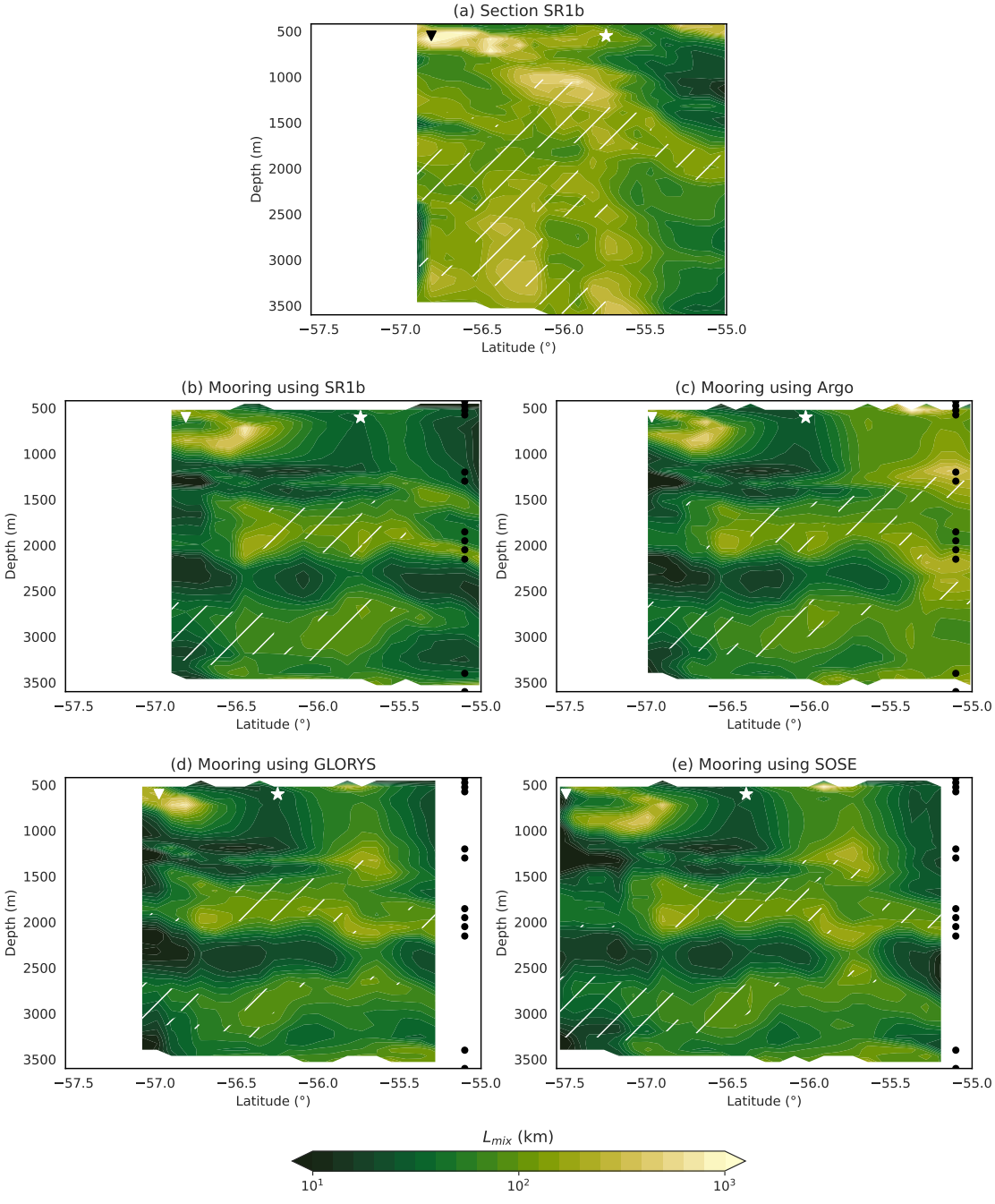

Figure B3. As Figure 5 but for L_{mix}.

https://doi.org/10.5194/egusphere-2026-2566
Preprint. Discussion started: 8 May 2026

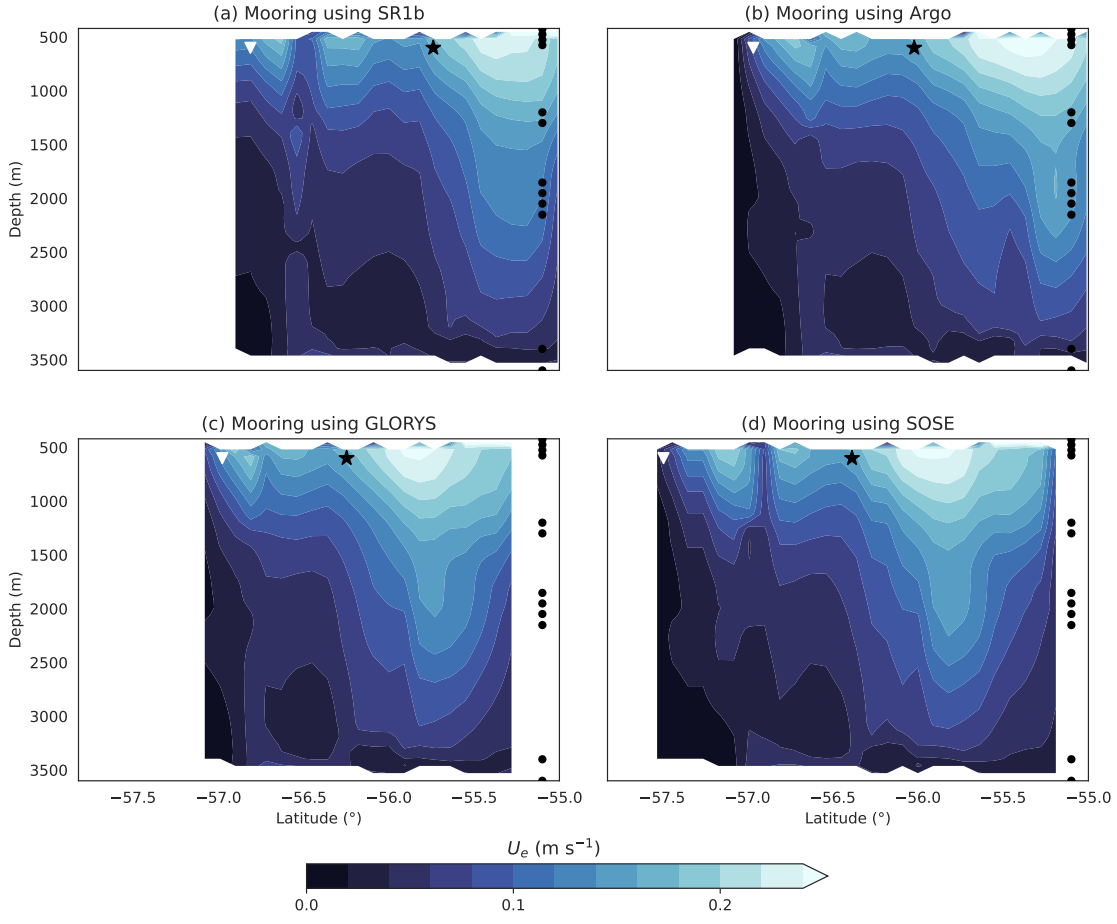

Figure B4. As Figure 5 but for U_e (only mooring data).

https://doi.org/10.5194/egusphere-2026-2566
Preprint. Discussion started: 8 May 2026

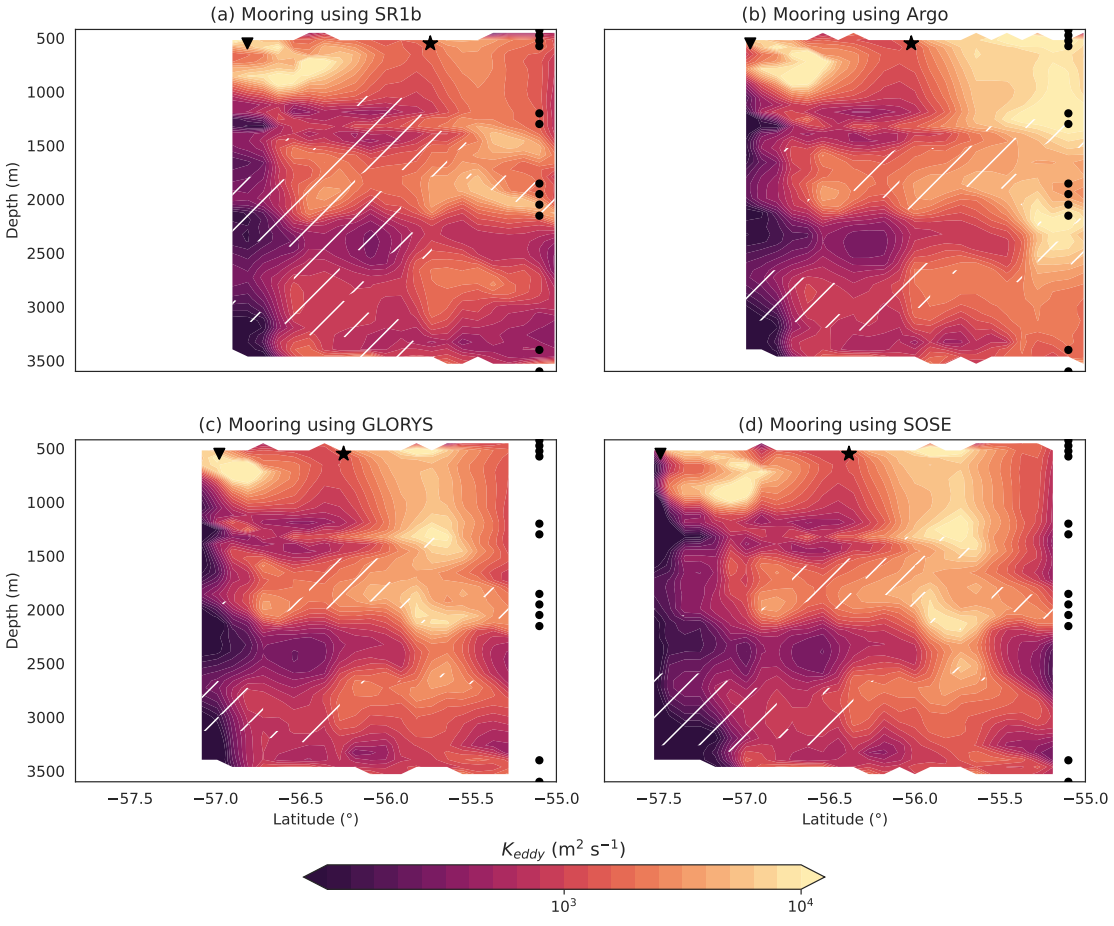

Figure B5. As Figure 5 but for $\mathcal{K}$ (only mooring data).

https://doi.org/10.5194/egusphere-2026-2566
Preprint. Discussion started: 8 May 2026

Author contributions. SG and ACNG conceptualised the original idea for this study. All co-authors contributed to developing the methodology. MFS and CJM carried out the analysis. MFS prepared the manuscript, with contributions from all co-authors. SG supervised the project.

Competing interests. SG is a member of the editorial board of Ocean Science.

Acknowledgements. We are grateful to Matthew Mazloff for providing the SOSE reanalysis data for us.

https://doi.org/10.5194/egusphere-2026-2566
Preprint. Discussion started: 8 May 2026

References

Abernathey, R., Marshall, J., Mazloff, M., and Shuckburgh, E.: Enhancement of Mesoscale Eddy Stirring at Steering Levels in the Southern Ocean, Journal of Physical Oceanography, 40, 170–184, https://doi.org/10.1175/2009JPO4201.1, 2010.

Abernathey, R., Marshall, J., and Ferreira, D.: The Dependence of Southern Ocean Meridional Overturning on Wind Stress, Journal of Physical Oceanography, 41, 2261–2278, https://doi.org/10.1175/JPO-D-11-023.1, 2011.

Abernathey, R. P. and Marshall, J.: Global Surface Eddy Diffusivities Derived from Satellite Altimetry, Journal of Geophysical Research: Oceans, 118, 901–916, https://doi.org/10.1002/jgrc.20066, 2013.

Armi, L. and Stommel, H.: Four Views of a Portion of the North Atlantic Subtropical Gyre, Journal of Physical Oceanography, 13, 828–857, https://doi.org/10.1175/1520-0485(1983)013<0828:FVOAPO>2.0.CO;2, 1983.

Balwada, D., Speer, K. G., LaCasce, J. H., Owens, W. B., Marshall, J., and Ferrari, R.: Circulation and Stirring in the Southeast Pacific Ocean and the Scotia Sea Sectors of the Antarctic Circumpolar Current, Journal of Physical Oceanography, 46, 2005–2027, https://doi.org/10.1175/JPO-D-15-0207.1, 2016.

Barker, P. M. and McDougall, T. J.: Two Interpolation Methods Using Multiply-Rotated Piecewise Cubic Hermite Interpolating Polynomials, Journal of Atmospheric and Oceanic Technology, 37, 605–619, https://doi.org/10.1175/JTECH-D-19-0211.1, 2020.

Brearley, J. A., Sheen, K. L., Naveira Garabato, A. C., Smeed, D. A., and Waterman, S.: Eddy-Induced Modulation of Turbulent Dissipation over Rough Topography in the Southern Ocean, Journal of Physical Oceanography, 43, 2288–2308, https://doi.org/10.1175/JPO-D-12-0222.1, 2013.

Brearley, J. A., Sheen, K. L., Naveira Garabato, A. C., Smeed, D. A., Speer, K. G., Thurnherr, A. M., Meredith, M. P., and Waterman, S.: Deep Boundary Current Disintegration in Drake Passage, Geophysical Research Letters, 41, 121–127, https://doi.org/10.1002/2013GL058617, 2014.

Busecke, J. J. M. and Abernathey, R. P.: Ocean Mesoscale Mixing Linked to Climate Variability, Science Advances, 5, eaav5014, https://doi.org/10.1126/sciadv.aav5014, 2019.

Chapman, C. and Sallée, J.-B.: Isopycnal Mixing Suppression by the Antarctic Circumpolar Current and the Southern Ocean Meridional Overturning Circulation, Journal of Physical Oceanography, 47, 2023–2045, https://doi.org/10.1175/JPO-D-16-0263.1, 2017.

Chen, R., Gille, S. T., McClean, J. L., Flierl, G. R., and Griesel, A.: A Multiwavenumber Theory for Eddy Diffusivities and Its Application to the Southeast Pacific (DIMES) Region, Journal of Physical Oceanography, 45, 1877–1896, https://doi.org/10.1175/JPO-D-14-0229.1, 2015.

Chouksey, A., Griesel, A., Chouksey, M., and Eden, C.: Changes in Global Ocean Circulation Due to Isopycnal Diffusion, Journal of Physical Oceanography, 52, 2219–2235, https://doi.org/10.1175/JPO-D-21-0205.1, 2022.

Cole, S. T., Wortham, C., Kunze, E., and Owens, W. B.: Eddy Stirring and Horizontal Diffusivity from Argo Float Observations: Geographic and Depth Variability, Geophysical Research Letters, 42, 3989–3997, https://doi.org/10.1002/2015GL063827, 2015.

Cusack, J. M., Brearley, J. A., Naveira Garabato, A. C., Smeed, D. A., Polzin, K. L., Velzeboer, N., and Shakespeare, C. J.: Observed Eddy–Internal Wave Interactions in the Southern Ocean, Journal of Physical Oceanography, 50, 3043–3062, https://doi.org/10.1175/JPO-D-20-0001.1, 2020.

De La Lama, M. S., LaCasce, J. H., and Fuhr, H. K.: The Vertical Structure of Ocean Eddies, Dynamics and Statistics of the Climate System, p. dzw001, https://doi.org/10.1093/climsys/dzw001, 2016.

https://doi.org/10.5194/egusphere-2026-2566
Preprint. Discussion started: 8 May 2026

Deng, P. and Wang, Y.: Distinct Impacts of Topographic versus Planetary PV Gradients on Baroclinic Turbulence, Journal of Physical Oceanography, https://doi.org/10.1175/JPO-D-24-0014.1, 2024.

Dettling, N., Nakayama, Y., Mensah, V., and Losch, M.: A Topography-Aware Eddy Parameterization Improves Warm Water Transport Across the Cape Darnley Continental Slope, Journal of Advances in Modeling Earth Systems, 17, e2025MS005 115, https://doi.org/10.1029/2025MS005115, 2025.

Ferrari, R. and Nikurashin, M.: Suppression of Eddy Diffusivity across Jets in the Southern Ocean, Journal of Physical Oceanography, 40, 1501–1519, https://doi.org/10.1175/2010JPO4278.1, 2010.

Ferrari, R. and Polzin, K. L.: Finescale Structure of the T–S Relation in the Eastern North Atlantic, Journal of Physical Oceanography, 35, 1437–1454, https://doi.org/10.1175/JPO2763.1, 2005.

Freeman, N. M., Lovenduski, N. S., and Gent, P. R.: Temporal Variability in the Antarctic Polar Front (2002–2014), Journal of Geophysical Research: Oceans, 121, 7263–7276, https://doi.org/10.1002/2016JC012145, 2016.

Gent, P. R. and McWilliams, J. C.: Isopycnal Mixing in Ocean Circulation Models, Journal of Physical Oceanography, 20, 150–155, https://doi.org/10.1175/1520-0485(1990)020<0150:IMIOCM>2.0.CO;2, 1990.

Gent, P. R., Willebrand, J., McDougall, T. J., and McWilliams, J. C.: Parameterizing Eddy-Induced Tracer Transports in Ocean Circulation Models, Journal of Physical Oceanography, 25, 463–474, https://doi.org/10.1175/1520-0485(1995)025<0463:PEITTI>2.0.CO;2, 1995.

Giglio, D. and Johnson, G. C.: Subantarctic and Polar Fronts of the Antarctic Circumpolar Current and Southern Ocean Heat and Freshwater Content Variability: A View from Argo, Journal of Physical Oceanography, 46, 749–768, https://doi.org/10.1175/JPO-D-15-0131.1, 2016.

Gille, S. T., Sheen, K. L., Swart, S., and Thompson, A. F.: Mixing in the Southern Ocean, in: Ocean Mixing, pp. 301–327, Elsevier, ISBN 978-0-12-821512-8, https://doi.org/10.1016/B978-0-12-821512-8.00019-0, 2022.

Gnanadesikan, A., Pradal, M.-A., and Abernathey, R.: Isopycnal Mixing by Mesoscale Eddies Significantly Impacts Oceanic Anthropogenic Carbon Uptake, Geophysical Research Letters, 42, 4249–4255, https://doi.org/10.1002/2015GL064100, 2015.

Griesel, A., Eden, C., Koopmann, N., and Yulaeva, E.: Comparing Isopycnal Eddy Diffusivities in the Southern Ocean with Predictions from Linear Theory, Ocean Modelling, 94, 33–45, https://doi.org/10.1016/j.ocemod.2015.08.001, 2015.

Griffies, S. M.: The Gent–McWilliams Skew Flux, Journal of Physical Oceanography, 28, 831–841, https://doi.org/10.1175/1520-0485(1998)028<0831:TGMSF>2.0.CO;2, 1998.

Groeskamp, S., Zika, J. D., Sloyan, B. M., McDougall, T. J., and McIntosh, P. C.: A Thermohaline Inverse Method for Estimating Diathermohaline Circulation and Mixing, Journal of Physical Oceanography, 44, 2681–2697, https://doi.org/10.1175/JPO-D-14-0039.1, 2014.

Groeskamp, S., Sloyan, B. M., Zika, J. D., and McDougall, T. J.: Mixing Inferred from an Ocean Climatology and Surface Fluxes, Journal of Physical Oceanography, 47, 667–687, https://doi.org/10.1175/JPO-D-16-0125.1, 2017.

Groeskamp, S., Barker, P. M., McDougall, T. J., Abernathey, R. P., and Griffies, S. M.: VENM: An Algorithm to Accurately Calculate Neutral Slopes and Gradients, Journal of Advances in Modeling Earth Systems, 11, 1917–1939, https://doi.org/10.1029/2019MS001613, 2019.

Groeskamp, S., LaCasce, J. H., McDougall, T. J., and Rogé, M.: Full-Depth Global Estimates of Ocean Mesoscale Eddy Mixing From Observations and Theory, Geophysical Research Letters, 47, 1–12, https://doi.org/10.1029/2020GL089425, 2020.

Hewitt, H. T., Roberts, M., Mathiot, P., Biastoch, A., Blockley, E., Chassignet, E. P., Fox-Kemper, B., Hyder, P., Marshall, D. P., Popova, E., Treguier, A.-M., Zanna, L., Yool, A., Yu, Y., Beadling, R., Bell, M., Kuhlbrodt, T., Arsouze, T., Bellucci, A., Castruccio, F., Gan, B., Putrasahan, D., Roberts, C. D., Van Roekel, L., and Zhang, Q.: Resolving and Parameterising the Ocean Mesoscale in Earth System Models, Current Climate Change Reports, 6, 137–152, https://doi.org/10.1007/s40641-020-00164-w, 2020.

https://doi.org/10.5194/egusphere-2026-2566
Preprint. Discussion started: 8 May 2026

Holloway, G.: Estimation of Oceanic Eddy Transports from Satellite Altimetry, Nature, 323, 243–244, https://doi.org/10.1038/323243a0, 1986.

Holmes, R. M., Groeskamp, S., Stewart, K. D., and McDougall, T. J.: Sensitivity of a Coarse-Resolution Global Ocean Model to a Spatially Variable Neutral Diffusivity, Journal of Advances in Modeling Earth Systems, 14, https://doi.org/10.1029/2021MS002914, 2022.

Howard, E., McC. Hogg, A., Waterman, S., and Marshall, D. P.: The Injection of Zonal Momentum by Buoyancy Forcing in a Southern Ocean Model, Journal of Physical Oceanography, 45, 259–271, https://doi.org/10.1175/JPO-D-14-0098.1, 2015.

Jackett, D. R. and McDougall, T. J.: A Neutral Density Variable for the World's Oceans, Journal of Physical Oceanography, 27, 237–263, https://doi.org/10.1175/1520-0485(1997)027<0237:ANDVFT>2.0.CO;2, 1997.

Jakes, M. I., Phillips, H. E., Cyriac, A., Foppert, A., Bindoff, N. L., Rintoul, S. R., and Polzin, K. L.: Thermohaline Interleaving in the Antarctic Circumpolar Current, Journal of Physical Oceanography, 55, 205–227, https://doi.org/10.1175/JPO-D-24-0048.1, 2025.

Jones, C. S. and Abernathey, R. P.: Isopycnal Mixing Controls Deep Ocean Ventilation, Geophysical Research Letters, 46, 13 144–13 151, https://doi.org/10.1029/2019GL085208, 2019.

Keffer, T. and Holloway, G.: Estimating Southern Ocean Eddy Flux of Heat and Salt from Satellite Altimetry, Nature, 332, 624–626, https://doi.org/10.1038/332624a0, 1988.

Kim, Y. S. and Orsi, A. H.: On the Variability of Antarctic Circumpolar Current Fronts Inferred from 1992–2011 Altimetry, Journal of Physical Oceanography, 44, 3054–3071, https://doi.org/10.1175/JPO-D-13-0217.1, 2014.

Klocker, A. and Abernathey, R.: Global Patterns of Mesoscale Eddy Properties and Diffusivities, Journal of Physical Oceanography, 44, 1030–1046, https://doi.org/10.1175/JPO-D-13-0159.1, 2014.

Klocker, A., Ferrari, R., and LaCasce, J. H.: Estimating Suppression of Eddy Mixing by Mean Flows, Journal of Physical Oceanography, 42, 1566–1576, https://doi.org/10.1175/JPO-D-11-0205.1, 2012.

Kusters, N., Groeskamp, S., and McDougall, T. J.: Spiralling Inverse Method: A New Inverse Method to Estimate Ocean Mixing, Journal of Physical Oceanography, 54, 2289–2309, https://doi.org/10.1175/JPO-D-24-0009.1, 2024.

Kusters, N., Balwada, D., and Groeskamp, S.: Global Observational Estimates of Mesoscale Eddy-Driven Quasi-Stokes Velocity and Buoyancy Diffusivity, Geophysical Research Letters, 52, e2025GL115 802, https://doi.org/10.1029/2025GL115802, 2025.

LaCasce, J. H. and Groeskamp, S.: Baroclinic Modes over Rough Bathymetry and the Surface Deformation Radius, Journal of Physical Oceanography, 50, 2835–2847, https://doi.org/10.1175/JPO-D-20-0055.1, 2020.

LaCasce, J. H., Ferrari, R., Marshall, J., Tulloch, R., Balwada, D., and Speer, K.: Float-Derived Isopycnal Diffusivities in the DIMES Experiment, Journal of Physical Oceanography, 44, 764–780, https://doi.org/10.1175/JPO-D-13-0175.1, 2014.

Ledwell, J. R., Watson, A. J., and Law, C. S.: Evidence for Slow Mixing across the Pycnocline from an Open-Ocean Tracer-Release Experiment, Nature, 364, 701–703, https://doi.org/10.1038/364701a0, 1993.

Ledwell, J. R., Watson, A. J., and Law, C. S.: Mixing of a Tracer in the Pycnocline, Journal of Geophysical Research: Oceans, 103, 21 499–21 529, https://doi.org/10.1029/98JC01738, 1998.

Marshall, J. and Radko, T.: A Model of the Upper Branch of the Meridional Overturning of the Southern Ocean, Progress in Oceanography, 70, 331–345, https://doi.org/10.1016/j.pocean.2006.07.004, 2006.

Marshall, J. and Speer, K.: Closure of the Meridional Overturning Circulation through Southern Ocean Upwelling, Nature Geoscience, 5, 171–180, https://doi.org/10.1038/ngeo1391, 2012.

Mazloff, M. R., Heimbach, P., and Wunsch, C.: An Eddy-Permitting Southern Ocean State Estimate, Journal of Physical Oceanography, 40, 880–899, https://doi.org/10.1175/2009JPO4236.1, 2010.

https://doi.org/10.5194/egusphere-2026-2566
Preprint. Discussion started: 8 May 2026

McDougall, T. J.: Potential Enthalpy: A Conservative Oceanic Variable for Evaluating Heat Content and Heat Fluxes, Journal of Physical Oceanography, 33, 945–963, https://doi.org/10.1175/1520-0485(2003)033<0945:PEACOV>2.0.CO;2, 2003.

McDougall, T. J. and Barker, P.: Getting Started with TEOS-10 and the Gibbs Seawater (GSW) Oceanographic Toolbox, SCOR/IAPSO WG127, ISBN 978-0-646-55621-5, 2011.

McDougall, T. J. and McIntosh, P. C.: The Temporal-Residual-Mean Velocity. Part II: Isopycnal Interpretation and the Tracer and Momentum Equations, Journal of Physical Oceanography, 31, 1222–1246, https://doi.org/10.1175/1520-0485(2001)031<1222:TTRMVP>2.0.CO;2, 2001.

McDougall, T. J., Jackett, D. R., Millero, F. J., Pawlowicz, R., and Barker, P. M.: A Global Algorithm for Estimating Absolute Salinity, Ocean Science, 8, 1123–1134, https://doi.org/10.5194/os-8-1123-2012, 2012.

McDougall, T. J., Groeskamp, S., and Griffies, S. M.: On Geometrical Aspects of Interior Ocean Mixing, Journal of Physical Oceanography, 44, 2164–2175, https://doi.org/10.1175/JPO-D-13-0270.1, 2014.

Meneghello, G., Marshall, J., Cole, S. T., and Timmermans, M.-L.: Observational Inferences of Lateral Eddy Diffusivity in the Halocline of the Beaufort Gyre, Geophysical Research Letters, 44, https://doi.org/10.1002/2017GL075126, 2017.

Meredith, M. P., Naveira Garabato, A. C., Hogg, A. M., and Farneti, R.: Sensitivity of the Overturning Circulation in the Southern Ocean to Decadal Changes in Wind Forcing, Journal of Climate, 25, 99–110, https://doi.org/10.1175/2011JCLI4204.1, 2012.

Nakamura, N. and Zhu, D.: Formation of Jets through Mixing and Forcing of Potential Vorticity: Analysis and Parameterization of Beta-Plane Turbulence, Journal of the Atmospheric Sciences, 67, 2717–2733, https://doi.org/10.1175/2009JAS3159.1, 2010.

Naveira Garabato, A. C., Stevens, D. P., Watson, A. J., and Roether, W.: Short-Circuiting of the Overturning Circulation in the Antarctic Circumpolar Current, Nature, 447, 194–197, https://doi.org/10.1038/nature05832, 2007.

Naveira Garabato, A. C., Jullion, L., Stevens, D. P., Heywood, K. J., and King, B. A.: Variability of Subantarctic Mode Water and Antarctic Intermediate Water in the Drake Passage during the Late-Twentieth and Early-Twenty-First Centuries, Journal of Climate, 22, 3661–3688, https://doi.org/10.1175/2009JCLI2621.1, 2009.

Naveira Garabato, A. C., Ferrari, R., and Polzin, K. L.: Eddy Stirring in the Southern Ocean, Journal of Geophysical Research: Oceans, 116, https://doi.org/10.1029/2010JC006818, 2011.

Naveira Garabato, A. C., Polzin, K. L., Ferrari, R., Zika, J. D., and Forryan, A.: A Microscale View of Mixing and Overturning across the Antarctic Circumpolar Current, Journal of Physical Oceanography, 46, 233–254, https://doi.org/10.1175/JPO-D-15-0025.1, 2016.

Newman, L., Heil, P., Trebilco, R., Katsumata, K., Constable, A., Van Wijk, E., Assmann, K., Beja, J., Bricher, P., Coleman, R., Costa, D., Diggs, S., Farneti, R., Fawcett, S., Gille, S. T., Hendry, K. R., Henley, S., Hofmann, E., Maksym, T., Mazloff, M., Meijers, A., Meredith, M. M., Moreau, S., Ozsoy, B., Robertson, R., Schloss, I., Schofield, O., Shi, J., Sikes, E., Smith, I. J., Swart, S., Wahlin, A., Williams, G., Williams, M. J. M., Herraiz-Borreguero, L., Kern, S., Lieser, J., Massom, R. A., Melbourne-Thomas, J., Miloslavich, P., and Spreen, G.: Delivering Sustained, Coordinated, and Integrated Observations of the Southern Ocean for Global Impact, Frontiers in Marine Science, 6, 433, https://doi.org/10.3389/fmars.2019.00433, 2019.

Olbers, D. and Visbeck, M.: A Model of the Zonally Averaged Stratification and Overturning in the Southern Ocean, Journal of Physical Oceanography, 35, 1190–1205, https://doi.org/10.1175/JPO2750.1, 2005.

Pennel, R. and Kamenkovich, I.: On the Factors Controlling the Eddy-Induced Transport in the Antarctic Circumpolar Current, Journal of Physical Oceanography, 44, 2127–2138, https://doi.org/10.1175/JPO-D-13-0256.1, 2014.

Pradal, M.-A. and Gnanadesikan, A.: How Does the Redi Parameter for Mesoscale Mixing Impact Global Climate in an Earth System Model?, Journal of Advances in Modeling Earth Systems, 6, 586–601, https://doi.org/10.1002/2013MS000273, 2014.

https://doi.org/10.5194/egusphere-2026-2566
Preprint. Discussion started: 8 May 2026

Prandtl, L.: Bericht Über Untersuchungen Zur Ausgebildeten Turbulenz, Zeitschrift für Angewandte Mathematik und Mechanik, 5, 136–139, 1925.

Redi, M. H.: Oceanic Isopycnal Mixing by Coordinate Rotation, Journal of Physical Oceanography, 12, 1154–1158, https://doi.org/10.1175/1520-0485(1982)012<1154:OIMBCR>2.0.CO;2, 1982.

Rintoul, S. R.: The Global Influence of Localized Dynamics in the Southern Ocean, Nature, 558, 209–218, https://doi.org/10.1038/s41586-018-0182-3, 2018.

Rintoul, S. R. and Naveira Garabato, A. C.: Dynamics of the Southern Ocean Circulation, in: International Geophysics, vol. 103, pp. 471–492, Elsevier, ISBN 978-0-12-391851-2, https://doi.org/10.1016/B978-0-12-391851-2.00018-0, 2013.

Roach, C. J., Balwada, D., and Speer, K.: Horizontal Mixing in the Southern Ocean from Argo Float Trajectories, Journal of Geophysical Research: Oceans, 121, 5570–5586, https://doi.org/10.1002/2015JC011440, 2016.

Roach, C. J., Balwada, D., and Speer, K.: Global Observations of Horizontal Mixing from Argo Float and Surface Drifter Trajectories, Journal of Geophysical Research: Oceans, 123, 4560–4575, https://doi.org/10.1029/2018JC013750, 2018.

Roemmich, D. and Gilson, J.: The 2004–2008 Mean and Annual Cycle of Temperature, Salinity, and Steric Height in the Global Ocean from the Argo Program, Progress in Oceanography, 82, 81–100, https://doi.org/10.1016/j.pocean.2009.03.004, 2009.

Sallée, J.-B., Speer, K., and Rintoul, S.: Mean-Flow and Topographic Control on Surface Eddy-Mixing in the Southern Ocean, Journal of Marine Research, 69, 753–777, https://doi.org/10.1357/002224011799849408, 2011.

Sallée, J.-B., Morrison, A. K., Naughten, K., and Thompson, A. F.: Southern Ocean Circulation, pp. 65–86, Routledge, London, 1 edn., ISBN 978-1-003-40647-1, https://doi.org/10.4324/9781003406471-4, 2025.

Sévellec, F., Naveira Garabato, A. C., Brearley, J. A., and Sheen, K. L.: Vertical Flow in the Southern Ocean Estimated from Individual Moorings, Journal of Physical Oceanography, 45, 2209–2220, https://doi.org/10.1175/JPO-D-14-0065.1, 2015.

Sévellec, F., Colin de Verdière, A., and Kolodziejczyk, N.: Estimation of Horizontal Turbulent Diffusivity from Deep Argo Float Displacements, Journal of Physical Oceanography, 52, 1509–1529, https://doi.org/10.1175/JPO-D-21-0150.1, 2022.

Smith, K. S. and Marshall, J.: Evidence for Enhanced Eddy Mixing at Middepth in the Southern Ocean, Journal of Physical Oceanography, 39, 50–69, https://doi.org/10.1175/2008JPO3880.1, 2009.

Srinivasan, K. and Young, W. R.: Reynolds Stress and Eddy Diffusivity of SS-Plane Shear Flow, Journal of the Atmospheric Sciences, 71, 2169–2185, https://doi.org/10.1175/JAS-D-13-0246.1, 2014.

Sterl, M. F., LaCasce, J. H., Groeskamp, S., Nummelin, A., Isachsen, P. E., and Baatsen, M. L. J.: Suppression of Mesoscale Eddy Mixing by Topographic PV Gradients, Journal of Physical Oceanography, 54, 1089–1103, https://doi.org/10.1175/JPO-D-23-0142.1, 2024.

Tulloch, R., Ferrari, R., Jahn, O., Klocker, A., LaCasce, J., Ledwell, J. R., Marshall, J., Messias, M.-J., Speer, K., and Watson, A.: Direct Estimate of Lateral Eddy Diffusivity Upstream of Drake Passage, Journal of Physical Oceanography, 44, 2593–2616, https://doi.org/10.1175/JPO-D-13-0120.1, 2014.

Vollmer, L. and Eden, C.: A Global Map of Meso-Scale Eddy Diffusivities Based on Linear Stability Analysis, Ocean Modelling, 72, 198–209, https://doi.org/10.1016/j.ocemod.2013.09.006, 2013.

Young, W. R.: An Exact Thickness-Weighted Average Formulation of the Boussinesq Equations, Journal of Physical Oceanography, 42, 692–707, https://doi.org/10.1175/JPO-D-11-0102.1, 2012.

Zika, J. D., McDougall, T. J., and Sloyan, B. M.: Weak Mixing in the Eastern North Atlantic: An Application of the Tracer-Contour Inverse Method, Journal of Physical Oceanography, 40, 1881–1893, https://doi.org/10.1175/2010JPO4360.1, 2010.